JGR Solid Earth

RESEARCH ARTICLE
10.1029/2021JB023858

Intra-Crater Eruption Dynamics at Nyiragongo (D.R. Congo), 2002–2021

Julien Barrière[1], Nicolas d'Oreye[1,2], Benoît Smets[3,4], Adrien Oth[1], Louise Delhaye[3,4], Josué Subira[5,6], Niche Mashagiro[5], Dominique Derauw[7,8], Delphine Smittarello[1], Adalbert Muhindo Syavulisembo[5], and François Kervyn[3]

[1]European Center for Geodynamics and Seismology, Walferdange, Luxembourg, [2]Department of Geophysics/Astrophysics, National Museum of Natural History, Luxembourg City, Luxembourg, [3]Natural Hazards Service, Department of Earth Sciences, Royal Museum for Central Africa, Tervuren, Belgium, [4]Cartography and GIS Research Group, Department of Geography, Vrije Universiteit Brussel, Ixelles, Belgium, [5]Goma Volcano Observatory, Goma, Democratic Republic of the Congo, [6]Department of Geography, Université de Liège, Liège, Belgium, [7]Centre Spatial de Liège, Liège, Belgium, [8]Laboratorio de Estudio y Seguimiento de Volcanes Activos, Instituto de Investigación en Paleobiología y Geología, Universidad Nacional de Rio Negro, General Roca, Argentina

Key Points:

- Processing of 1,703 satellite radar images leads to the first reliable picture of erupted volumes within Nyiragongo's crater since 2002
- We provide a multi-instrumental analysis with topographic reconstructions using photogrammetry and seismic observations at Nyiragongo
- Our approach helps to decipher the origins of surface (intra-crater) evidences of magmatic pressure variations in the plumbing system

Supporting Information:

Supporting Information may be found in the online version of this article.

Correspondence to:

J. Barrière,
julien.barriere@ecgs.lu

Citation:

Barrière, J., Nicolas d'Oreye, Smets, B., Oth, A., Delhaye, L., Subira, J., et al. (2022). Intra-crater eruption dynamics at Nyiragongo (D.R. Congo), 2002–2021. *Journal of Geophysical Research: Solid Earth*, *127*, e2021JB023858. https://doi.org/10.1029/2021JB023858

Received 18 DEC 2021
Accepted 26 MAR 2022

Abstract Nyiragongo is one of the rare volcanoes on Earth hosting a lava lake. However, the understanding of its plumbing and lava lake systems remains limited, with, until recently, only sporadic or time-limited historical observations and measurements. Combining dense accurate lava lake and crater floor level measurements based on 1,703 satellite radar images and topographic reconstructions using photogrammetry, we obtain the first reliable picture and time evolution of intra-crater erupted lava volumes between the two last flank eruptions in January 2002 and May 2021. The filling of the crater by lava, initiated in 2002 and continued up to May 2021, is seen as an evidence of a long-term pressure build up of the magmatic system. This filling occurs through irregular pulsatory episodes of rising lava lake level, some of which overflow and solidify on the surrounding crater floor. Pauses of stable molten lava lake level and sudden numerous level drops also marked the summit's eruptive activity. The joint analysis with seismic records available since 2015 revealed that the largest lava lake drops are synchronous with seismic swarms associated with deep magma intrusions, generally preceded by an increase of extrusion rate within the crater. The appearance of a spatter cone in the summit crater in 2016, most likely superficially branched to the lava lake, was a clear marker of the change in eruption dynamics. This first long-term time series of Nyiragongo's crater topography between two hazardous flank eruptions might further help to better decipher Nyiragongo's past and future behavior using multi-parameter observations.

Plain Language Summary Nyiragongo volcano, in D.R. Congo, stands close to a densely populated area (~1 million inhabitants). Its Hawaiian-style eruptive activity essentially consists in a long-lived molten lava lake or lava fountains in the summit crater lasting for weeks to decades, interrupted by effusive flank eruptions. Nyiragongo erupted on its southern flank in January 2002 and May 2021, draining the lava lake system and opening fissures producing rapid lava flows toward the city of Goma and Lake Kivu. Between these two flank eruptions, the continuous summit eruptive activity took the form of a persistent lava lake progressively filling in the summit crater. Here, we derive accurate elevation measurements of Nyiragongo's crater floor and lava lake surface between the two last flank eruptions from radar satellite instruments and 3D photogrammetric reconstruction. The lava lake, of which the level fluctuates, acts as a growing piezometer connected to the magmatic system as its rim rose by ~300 m in about 19 years due to overflowing. A combined analysis with seismic records provides important indications on the origins of the observed variations and helps to better understand the link between the continuous eruptive activity and the deeper magmatic processes.

1. Introduction

Nyiragongo volcano (D.R. Congo), 3,470 m a.s.l., located in the Virunga Volcanic Province (VVP) along the western branch of the East African rift, is one of the few volcanoes on Earth that several times has hosted a lava lake with decadal persistence, here inside the ~1.2-km wide summit crater (Lev et al., 2019; Figure 1a). Flank eruptions and associated drainage of its lava lake occurred at least three times, in January 1977, January 2002, and May 2021 (Global Volcanism Program, 2021; Komorowski et al., 2002; Pottier, 1978). These drainages led

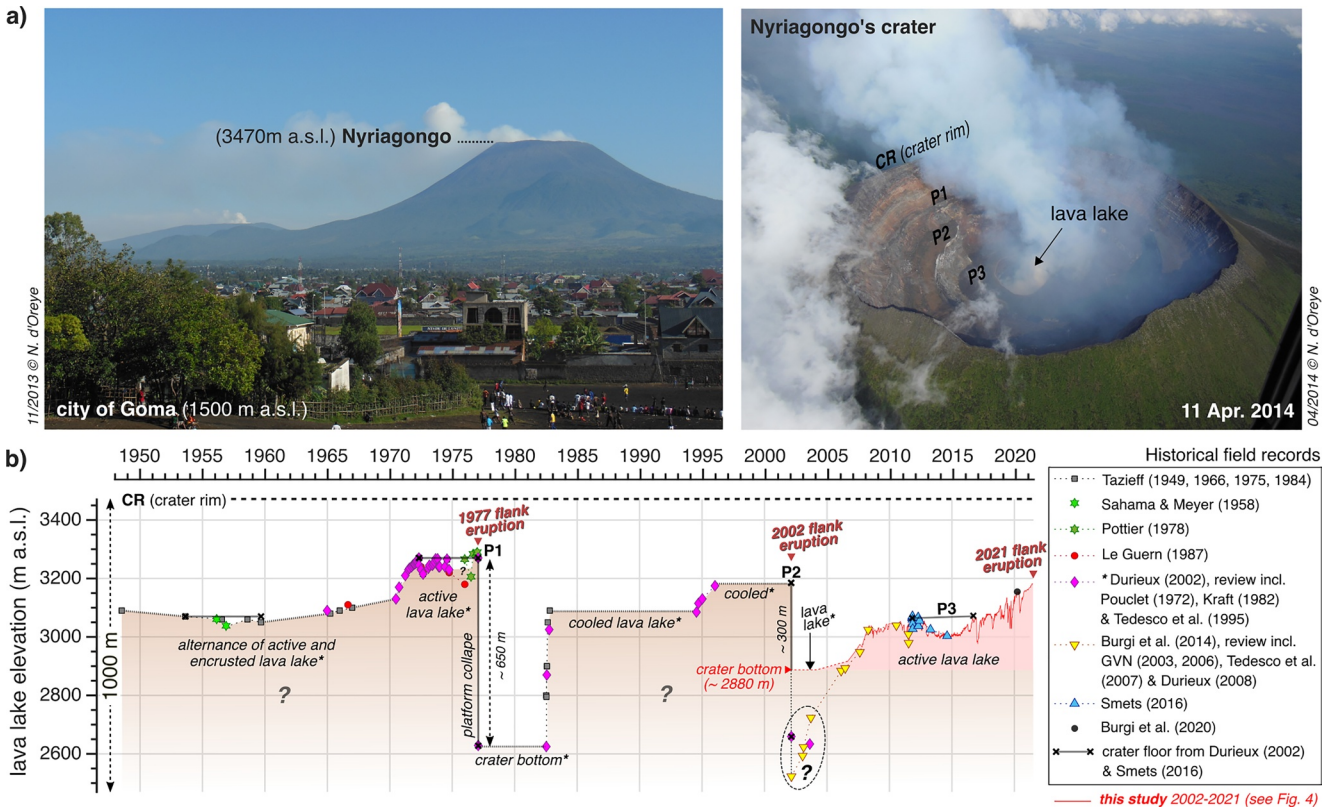

Figure 1. (a) Picture of Nyiragongo taken from the Goma Volcano Observatory (GVO) in November 2013. The active volcano Nyamulagira (D.R. Congo, ~3,058 m a.s.l.) is also visible at the background. The orientation of this picture is roughly South to North. An aerial view of Nyiragongo's crater in April 2014 is depicted on the right. (b) Lava lake elevation (in m a.s.l.) from historical field records and recent expeditions (1948–2020) and from the continuous estimates obtained in the present study (red line). Details about the references before 2016 can be found in Smets (2016). Comments marked by an asterisk come from the review paper by Durieux (2002). The new estimate of the crater floor after the 2002 eruption (~2,880 m a.s.l.) is taken into account (Section 3.1). Batches of former crater floor left after the 1977 eruption are named *P1* platform (~3,270 m a.s.l), while batches of level reached before the 2002 eruption are named *P2* platform (~3,185 m a.s.l). *P3* platform is the crater floor hosting the lava lake.

to collapses of the crater floor during the days following the flank eruptions. After the 2002 eruption, effusive activity within the crater resumed around May 2002 (Wright & Flynn, 2003) and has persisted and evolved ever since to the last May 2021 eruption. The altitude of the crater floor reached before the 2021 eruption is approximately similar to the level attained more than 6 years before the eruption in 2002 (i.e., ~3,185 m a.s.l.), and this level is about 85 m lower than the level reached before the first documented flank eruption at Nyiragongo in 1977 (Figure 1b). Despite the importance of understanding these lava lake and crater floor level changes and their evident relation with pressure variations in the magmatic system (e.g., Barrière et al., 2019; Burgi et al., 2014), height estimates mentioned in the literature were so far only obtained from the summit during short-term expeditions, often through measurements of rough or unknown precision (Figure 1b).

Here, we build high-temporal-resolution time series of lava lake and crater floor level measurements (sub-weekly at best) from several SAR (Synthetic Aperture Radar) sensors orbiting the Earth. An essential property of the SAR signal is that the radar beam along a line of sight is following a path that can be considered as a straight line independent of the time of acquisition, weather conditions, or presence of volcanic gas plume. Like the Sun's illumination, the SAR ray paths are obstructed by subvertical man-made or natural structures, and the shadow cast by the structure is proportional to its height (e.g., Brunner et al., 2010; Tapete et al., 2016). SAR amplitude images are in a specific projection called "slant range plane," which allows converting shadow length into true height changes through a straightforward geometric calculation (Figure 2).

Such a simple methodology has been already applied at African lava lake volcanoes Nyiragongo (Barrière et al., 2018) and Erta' Ale (Moore et al., 2019), giving the depth relative to the rim of the pit crater hosting both lava lakes. Following these studies, we have developed a semi-automatic processing that greatly improves the use

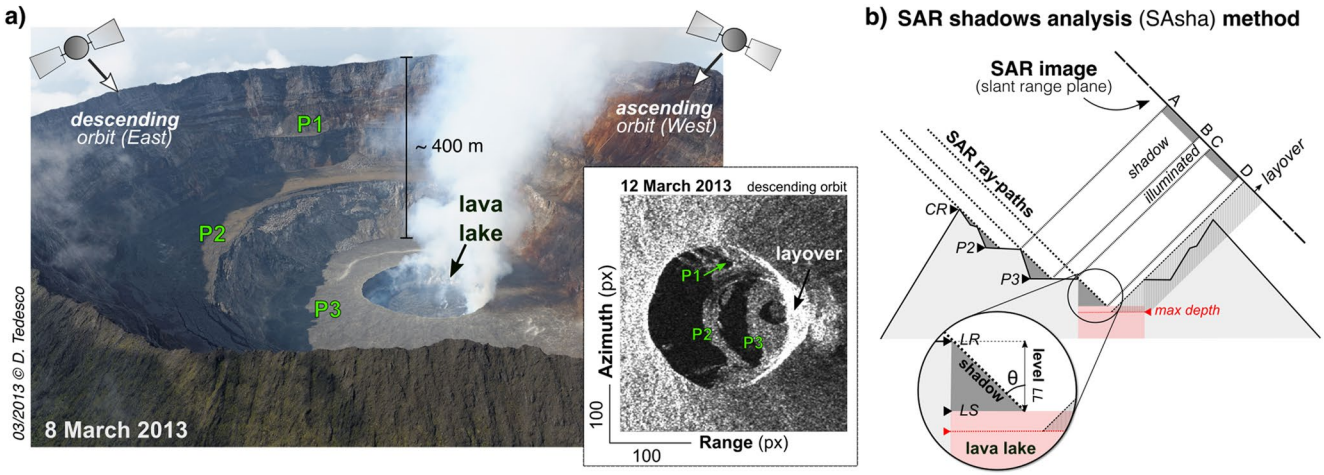

Figure 2. (a) Aerial picture of Nyiragongo's crater taken on 8 March 2013 (courtesy of D. Tedesco) illustrating the view angle from the ascending and descending orbits of the SAR satellites. The SAR amplitude image (RADARSAT-2) obtained 4 days later along the descending orbit is plotted. (b) Sketch of the cross section of Nyiragongo's crater explaining the principle of the SAsha method. For some unfavorable SAR geometries, the layover effect due to the backscattered signal from the opposite crater wall hampers the determination of the targeted points (*P3*, *LR*, or *LS*).

of SAR shadows for detecting Nyiragongo's lava lake and crater topography changes, leading to a comprehensive time series encompassing 15 years (May 2006–2021). The continuous SAR data set (1,703 images since 2006) is complemented by an isolated SAR image on December 26, 2003 and photogrammetry measurements on January 31, 2002 (14 days after the eruption on January 17, 2002) and August 8, 2016. Adding the in-field information of seismicity beneath Nyiragongo to this dense SAR-based time series allows us to unravel the origins and dynamics of the major pressure changes by connecting the surface lava accumulation and lava-lake-level fluctuations to deep (>10 km b.s.l.) or shallow magmatic processes. While the detailed mechanisms of the most recent May 2021 eruption remain beyond the scope of this paper, the present work provides an in-depth discussion about the magmatic processes behind the main crater topography changes observed during the ~19-year-long intra-crater eruptive activity interrupted by this last flank eruption.

2. Joint Space-Based and Ground-Based Approach

2.1. Crater Topography Changes Detected With SAR Shadows

The SAR-based technique SAsha (standing for SAR shadows analysis) has been developed for detecting changes in Nyiragongo's crater topography on a sub-weekly basis. The core product of the SAsha method is the length of SAR shadows computed along the range direction from SAR amplitude images, which are pre-processed with the C/C++/shell-based tool MasTer (InSAR automated Mass processing Toolbox for multidimensional Time series; e.g., Derauw et al., 2020; d'Oreye et al., 2021). For each SAR data set (i.e., same SAR sensor in same geometry), the two key processing steps are (1) denoising the raw amplitude images and (2) converting shadow lengths into height changes. Each image has a variable signal-to-noise ratio (SNR) and the boundaries of shadow areas can be more or less blurry, which, in turn, lowers the accuracy of the method consisting in picking the edges between illuminated and shadow areas. As the image processing method in step 1, we adopt the popular Rudin-Osher-Fatemi (ROF) total variation (TV) model (Rudin et al., 1992), which produces the denoised image given by (e.g., Micchelli et al., 2011):

$$\arg\min_{u} \left\{ \frac{1}{2} \|u - x\|_2^2 + \mu \|u\|_{TV} \right\}, \quad (1)$$

where x is the noisy image, u is the denoised image, μ is the regularization parameter, and $\|u\|_{TV}$ is the TV of u. This optimization problem is solved using the effective iterative Split-Bregman algorithm proposed by Goldstein and Osher (2009). In contrast with standard smoothing techniques (e.g., median filtering), this superior processing approach preserves the edges between contrasted regions while the amount of noise removal is tuned with the regularization parameter. Step 2 is the final shadow-to-height conversion, where we aim to determine the absolute

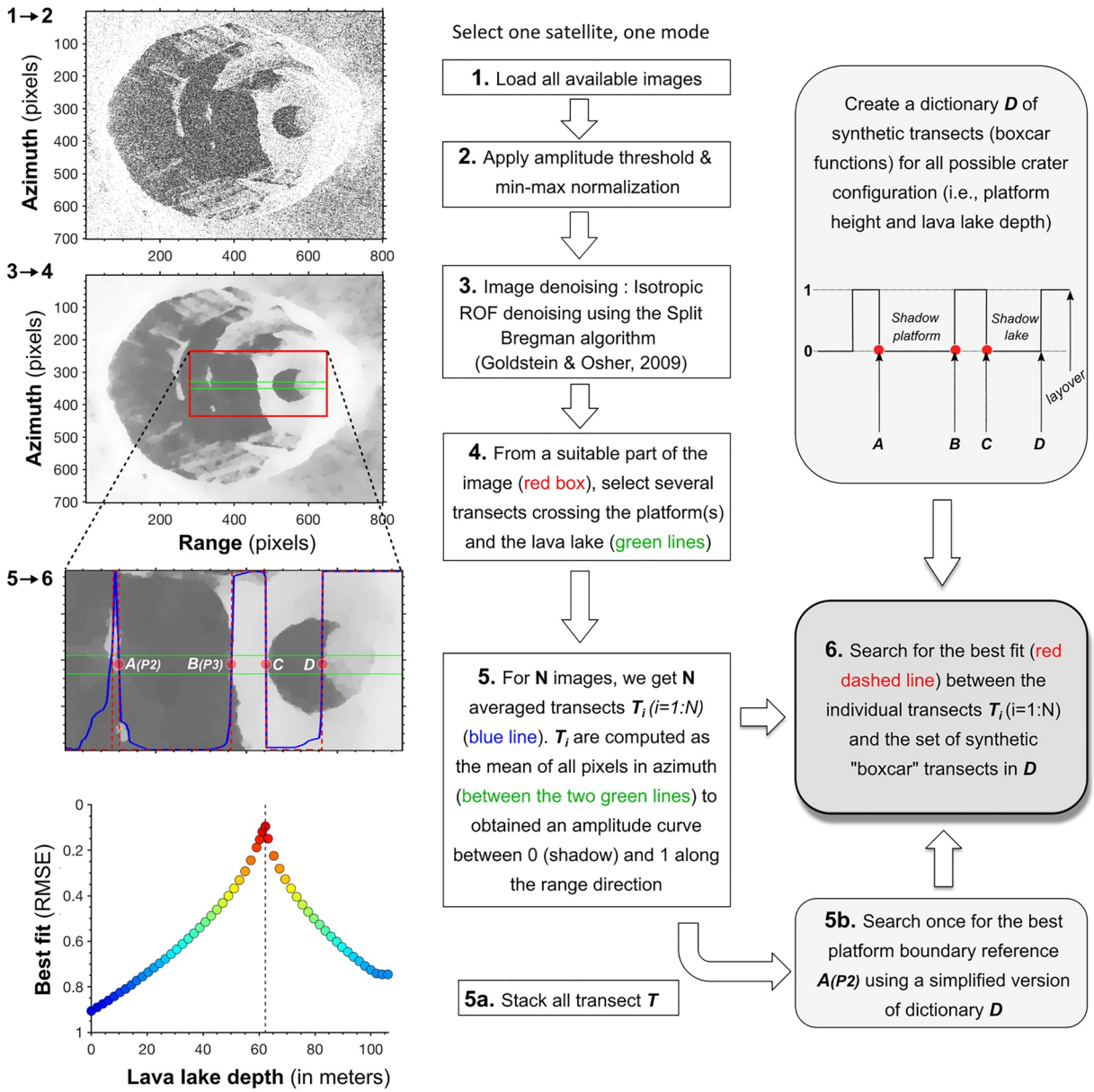

Figure 3. Flowchart (steps 1–6) of the SAsha method. The illustrative SAR image is the one obtained on August 25, 2014 with COSMO-SkyMed in ascending mode. On the western side, a remaining piece of platform *P2* can be used as reference.

altitude of the crater bottom (the platform $P3$, the lava lake rim LR, and the lava lake surface LS, see Figure 2b). To do so, we need to take into account the non-uniform lava accumulation over $P3$, due to the irregular effusive activity from a spatter cone that formed since February 29, 2016 (Balagizi et al., 2016). Therefore, a differential elevation between the illuminated points on $P3$ and the lava lake rim LR must be considered. For each SAR data set, all N images are sorted by date and processed iteratively to determine the independent rise of both $P3$ and the lava lake rim LR, and consequently LS. From Figures 2b and 3, we derive:

$$\text{for } i = 1{:}N, \begin{cases} P3_i = \text{Ref} - |AB_i| \times \cos\theta \times \text{resolution}, \\ LR_i = P3_1 + |C_iC_1| \,/\, \cos\theta \times \text{resolution}, \\ LS_i = LR_i - |C_iD_i| \times \cos\theta \times \text{resolution}, \end{cases} \tag{2}$$

where the fixed, absolute reference altitude Ref is either $P2$ or CR (crater rim) depending on the SAR angle (Figure 2b). The main assumption is that the altitudes of $P3$ and LR are identical for the first image ($i = 1$), which seems reasonable since all SAR datasets start well before the appearance of the spatter cone. The flowchart presented in Figure 3 summarizes the overall image processing of each SAR image to obtain the final elevation estimates $P3$, LR, and LS. The simpler equation applied by Barrière et al. (2018) at Nyiragongo and Moore et al. (2019) at Erta' Ale reduces to:

$$\text{for } i = 1{:}N, \quad LL_i = -|C_i D_i| \times \cos\theta \times \text{resolution}, \tag{3}$$

where LL_i is the lake's surface level (differential elevation between the lake rim and the lake surface expressed in negative values). In Moore et al. (2019), we note, however, that this equation may not have been formulated using the pixel spacing in slant range plane but in the geocoded image (see determination of SAR shadow in Figure 6 of Moore et al. [2019]). Here we must measure the shadow on images in slant range geometry to avoid propagating errors related to the geocoding on an outdated DEM, that is, that does not take into account the topographic changes that we measure.

The determination of shadow lengths has been automated using a dedicated dictionary-matching algorithm (Figure 3), but all results presented here have been manually checked and corrected if needed (about 1/3 of the full data set). Most errors consist in a few pixels shift but are sometimes more significant when the lava lake is overflowing over successive images. In that case, the automatic determination of C_i (the edge between the illuminated platform $P3$ and the lava lake shadow) becomes more uncertain (see eq. 2). Finally, depending on the diameter of the pit crater hosting the lava lake, the signal backscattered from the opposite crater wall can be received before that from the lava lake surface. This so-called "layover" effect (e.g., Pinel et al., 2014) imposes a maximum measurable lava lake depth and, depending on the angle and the satellite mode, can also prevent any determination of lava lake's attributes LR and LS. Over successive SAR images, there is also a potential trade-off between the variations of the diameter and the elevation of the pit crater, but we verified that this effect can be neglected (see Text S1 in Supporting Information S1).

Using the SAsha method, we processed 1,703 SAR images acquired by the satellites Sentinel-1 A/B, COSMO-SkyMed, RADARSAT-2, and ENVISAT, along several ascending and descending orbits, using different meter-scale resolutions and different overlapping time periods (see Table S1 in Supporting Information S1). We used the whole data set to estimate the depth of the crater (variations of $P3$) between May 19, 2006 and May 21, 2021. Due to the layover effect, 1,189 (70%) and 1,130 (66%) images can be used for estimating the elevation of the lava lake's rim LR and the lava lake's surface LS, respectively. Only 10 out of 1130 images give an estimate of the lava lake depth potentially affected by the layover effect (see Section 3.2 and Figure 4). An additional qualitative cross-checking with field pictures available on social networks has also been performed when their dates can be confirmed through the visitors' book of Virunga National Park.

2.2. Topographic Reconstructions Using Photogrammetry Measurements

We apply structure-from-motion photogrammetry principles to multispectral IKONOS satellite images acquired on January 31, 2002 and a series of optical unoccupied aerial vehicle (UAV) footages from August 8, 2016 during an expedition at the summit. The IKONOS-based measurement allows us to determine some essential geometrical properties of Nyiragongo's crater only 9 days after the 2002 collapse (Durieux, 2002). The UAV data from August 2016 provide optimal coverage of the crater, leading to a high-resolution 3D digital elevation model (DEM) for this date.

The photogrammetric processing workflow is performed with Agisoft Metashape Pro v. 1.6.5. The different processing steps follow those classically used in Structure-from-Motion photogrammetry, that is, (a) the photo alignment during which both interior and exterior orientations are estimated, (b) the georeferencing and the optimization of the estimated orientations, using ground control points (GCPs) and the tie point filtering options offered by the software, (c) the dense matching that produces a 3D dense point cloud, and (d) the production of a DEM based on a manually cleaned dense point cloud. The UAV-based data set was georeferenced with GCPs acquired in the field using differential GNSS. For the processing of the IKONOS images, no GCP is available, which leads to poor horizontal accuracy of georeferencing. The georeferencing is complemented via the use of

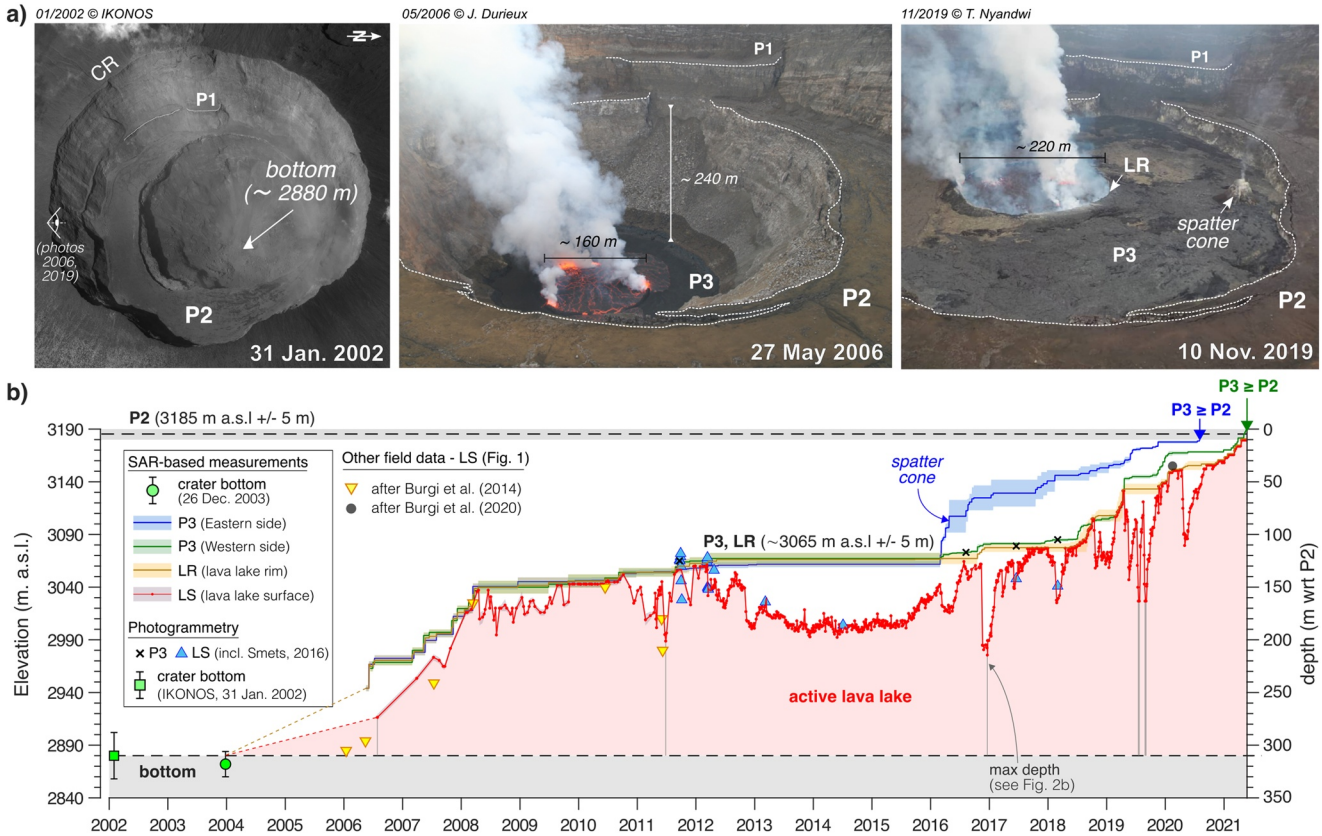

Figure 4. (a) A single IKONOS image acquired on January 31, 2002, 9 days after the crater collapse, and 14 days after the flank eruption. Two pictures of Nyiragongo's inner crater over a span of 13 years, on May 27, 2006 (courtesy of J. Durieux) and November 10, 2019 (courtesy of T. Nyandwi). (b) Topographic changes at Nyiragongo's crater: altitude of crater floor (*P3*), lava Lake Rim (*LR*), and lava Lake Surface (*LS*). Shaded area around satellite measurements' curves corresponds to error margins. Photogrammetry-based lava lake and *P3* level measurements (Smets, 2016; this study) are plotted with blue triangles and cross symbols, respectively. The elevations of the crater bottom estimated on January 31, 2002 and December 26, 2003 (see Section 3.1) are depicted as round and square green markers with error bars, respectively. Estimates from Burgi et al. (2014, 2020) are plotted with yellow inverted triangles and a black round marker (note that four of the six points from 2006 to 2010 have a coarse monthly temporal resolution, see also Text S3 in Supporting Information S1).

the rational polynomial coefficients (RPCs) file as input for the empirical modeling of the IKONOS pushbroom sensor (Agisoft LLC, 2020). This approach is often considered as an accurate alternative to a more time-consuming and mathematically complex physical modeling of the sensor (e.g., Rupnik et al., 2016, 2018). Table S2 in Supporting Information S1 provides the technical specifications of the UAV and IKONOS image acquisitions and the accuracy of the derived DEMs. The accuracy of georeferencing for the IKONOS DEM was estimated by comparing the five similar stable parts of the Nyiragongo crater between the IKONOS DEM and the UAV DEM. This comparison shows that we indeed have a poor accuracy of about 250 m in horizontal dimension, while much better accuracy of about 22 m in vertical.

2.3. Seismic Event Locations in the Virunga Volcanic Province

Since October 2015, between 7 and 14 seismic stations from the KivuSNet network (Oth et al., 2017) have been operational in the vicinity of Nyiragongo (<50 km). Before the deployment of a permanent seismic station on the main crater rim in March 2018, the closest station to the lava lake (KBTI) was located about 6 km away along the southeastern flank of the volcano.

The local KivuSNet seismic network, initially developed through research-based initiatives, rapidly emerged as the main monitoring tool for the Goma Volcano Observatory (GVO) since its design allows for efficient real-time seismic data access and routine analysis. For the particular periods of large fluctuations of the lava lake level, we

analyze later, in Sections 3.5 and 4.1, seismic events in the VVP are detected and located using a source-scanning method, providing automatic location solutions adapted to low SNR and low magnitude events typical of volcanic environments (e.g., Barrière et al., 2018; Poiata et al., 2016). Traditional routine location methods are based on iterative linearized inversion of travel-time data using manual or automatic arrival time picking of P-wave and/or S-wave onsets. In contrast, the "picking-free", cross-correlation-based technique we apply here uses a direct grid-search strategy, the details of which are provided in the Supporting Information (Text S2 in Supporting Information S1). An example of automatic location of a seismic event beneath Nyiragongo obtained with this dedicated location method (XCloc, standing for cross-correlation locator) is also given in Figure S3 in Supporting Information S1.

3. Time-Dependent Record of Intra-Crater Topography and Lave Lake Level

3.1. How Deep Was the Inner Crater After the 2002 Collapse?

It is well-known that the crater floor altitude prior the flank eruption on 17 January 2002 was about 3,185 m a.s.l. (platform *P2*, see Figure 1) but there are still large uncertainties about its depth after the crater collapsed 5 days later on January 22 (Durieux, 2002). Here, we incorporate into the analysis an isolated SAR amplitude image from December 26, 2003 (ENVISAT satellite) and the space-based photogrammetric result from January 31, 2002 (IKONOS satellite). Since no major changes occurred inside the crater between January 2002 and August 2005 (Balagizi et al., 2016), these two observations may give us a reliable estimate of the minimum altitude of the crater bottom right after the large collapse on January 22, 2002. Both SAR and photogrammetric measurements lead to a similar altitude of 2,872 ± 12 m a.s.l. (Figure S2 in Supporting Information S1) and 2,880 ± 22 m a.s.l (Table S2 in Supporting Information S1), respectively. Using the value of 2,880 m a.s.l, the 2002 collapse thus resulted in a ∼590-m deep subconical crater from the maximum elevation of the crater rim (3,470 m a.s.l.).

That depth allows estimating extruded volumes of lava within the crater since the 2002 eruption (see Section 3.3). This new measurement, confirmed by two independent observations, also answers to a long-standing debate that was at the origin of large and recurrent discrepancies found in the literature, for example, Durieux (2002), Tedesco et al. (2007), followed by Burgi et al. (2014, 2018, 2020) and relayed in a recent review article of Pouclet and Bram (2021). Presumably based on visual inspection, no information about the measurement methods nor uncertainty are given in the above-mentioned studies. Durieux (2002) indeed suggests a depth of 810 m compared to the maximum summit point (3,470 m a.s.l.) following the 2002 eruption or a depth of 835 m in July 2003, while Tedesco et al. (2007) estimate a depth of 945 m compared to the same maximum altitude (i.e., 2,525 m a.s.l), that is 355 m deeper than the maximum crater depth measured here (see Figure 1b).

3.2. Deriving Consistent Crater Topography Changes

With the available SAR data set, we are able to provide a precise picture of Nyiragongo's crater topography changes since May 2006. Considering the set of eq. 1, a final decisive step is to merge the total of 34 individual time series for $P3$, LR and LS obtained from different satellites (Table S1 in Supporting Information S1). First, we have to define the reference altitudes Ref (either the crater rim CR or the platform $P2$, Figure 2). Typical values for the crater rim range between 3,425 m (south-east reference, summit camp of Virunga National Park) and 3,470 m a.s.l. (highest point), while $P2$ is generally considered to be between ∼3,180 and 3,190 m on the eastern side and ∼3,190 m for pieces of the remaining platform on the western side (Smets, 2016). Accurate photogrammetric field measurements taken between September 2011 and March 2018 are useful for constraining our results (Smets, 2016; this study, Figure 4). We define the following reference values ranging in these intervals, best fitting this set of field measurements:

1. CR (crater rim): Between 3,445 and 3460 m a.s.l. in ascending (West) mode. Not used in descending mode.
2. $P2$ (edge of platform): 3,190 m a.s.l. for ascending mode (West), 3,180 m a.s.l. for descending mode (East).

It is noteworthy that the same values are used for satellites sharing the same reference points on $P2$ (e.g., $P2$ = 3,180 m for the five time series using satellite sensors in descending mode). Reference values for CR correspond to time series with the poorest range/height resolution (>5 m, ENVISAT, see Table S1 in Supporting

Information S1) and are adjusted accordingly to overlapping timeseries using *P2* as reference points. This leads to a shift in the reference points for *CR* within an interval of 15 m (3,445–3,460 m) for four ENVISAT time series acquired on the ascending orbit (western side). For each set of similar measurements (i.e., *P3* western side, *P3* eastern side, *LR*), we apply a uniformization of all single curves (including error margins) using a nearest-neighbor interpolation. The merging of all individual SAR-based measurements from different sensors is done by averaging these interpolated time series. As final conservative error margins, the uncertainty displayed in Figure 4b as shaded areas corresponds to the overall uncertainty (i.e., minimum to maximum) encompassing all individual SAR measurements that must be merged together. These errors might be potentially significant since, for the same target (i.e., *P3* or *LR*), each SAR sensor illuminates different points on a nonplanar surface and at irregular (non-daily) time intervals. However, after the daily interpolation of the maximum and minimum bounds, the final result displayed in Figure 4 shows a total daily error for *P3* western side, *P3* eastern side and *LR* below 10 m on average. This satisfactory uncertainty is an important confirmation of the quality of the results thanks to a very good agreement between the 23 time series (*P3* and *LR*) during overlapping periods. Since 2016, the largest uncertainty on the descending side for *P3* (up to 30 m) is due to the appearance of the spatter cone, where the SAR signal from COSMO-SkyMed, Sentinel-1, and RADARSAT-2 illuminate slope points on the cone at different elevations.

Because we subtract the height corresponding to the lake shadow from *LR* to determine the absolute lava-lake level *LS*, we cannot have two (western and eastern) estimates for *LR*. This would indeed imply that we have two different estimates for the lava lake's surface *LS*. Thus, we also average the two time series for *LR* and keep the minimum and maximum estimates as error margins. After the cone's appearance in March 2016, we only keep the western estimate of *LR*, which remains largely unaffected by the bulging of the rim on the eastern side due to cone's lava flows and thus best corresponds to the true elevation of the lava-lake rim (i.e., $LR - LS = 0$ when the lava lake is entirely filled). Contrary to *P3* and *LR*, *LS* often varies substantially between two SAR measurements, so we neither interpolate nor smooth the estimates obtained from different satellites. We can observe that the final *LS* time series (red curve in Figure 4b) exhibits coherent level estimates when results from multiple satellite sensors are mixed (e.g., the "quiescent" period 2013–2015). To summarize, the final composite result is depicted in Figure 4b as four elevation estimates:

1. *P3* measured on its eastern side (where the spatter cone appeared in 2016),
2. *P3* measured on its western side,
3. *LR*, which is an average between the western and eastern sides of the rim before March 2016, and
4. *LS*, the lava-lake surface.

Note that the resolution for the (relative) lava lake depth (i.e., *LL* in eq. 3) is about ±1.5 m (i.e., ±1 pixel) since 2012. For both *P3* and *LS*, the fit to the photogrammetric data is very satisfying, while very short-term variations (<1 day) measured in 2011 and 2012 (Smets, 2016) cannot be captured by the SAR method. Lava-lake-level data coming from different sources are reported by Burgi et al. (2014, 2018, 2020) for constraining a magma flow model at Nyiragongo. Between 2002 and 2003, these estimates are, by far (>150 m), below the minimum crater altitude measured in this study (see Figures 1b and Section 3.1). Between 2006 and 2011, six measurements agree with the SAR time series provided in our study. Among these six points, three were obtained by infrared laser rangefinder during expeditions in 2010 and 2011 (Burgi et al., 2014). From a field survey in February 2020, Burgi et al. (2020) estimated an altitude for the lava lake of 3,155 m a.s.l, which agrees well with our measurement for *LR* at the same date. Other data points reported by Burgi et al. (2018, 2020) exhibit numerous discrepancies, so we decided to not consider these data in the present study (they are plotted in Figure 5c alongside our results for comparison purpose only). We provide, however, a more detailed investigation of these data issues in Text S3, Figure S4, Tables S3–S4 in Supporting Information S1.

3.3. Temporal Evolution of Extruded Magma Volumes

Combining information retrieved from the space-based SAR and photogrammetry results (Sections 3.1 and 3.2) with the DEM obtained from the UAV-based photogrammetry in 2016, we can attempt a first cross-section representation of Nyiragongo's crater as presented in Figures 5a and 5b. For the sake of simplification, the lava lake shape is plotted along a fixed centered position even though it has probably deviated to a small extent over

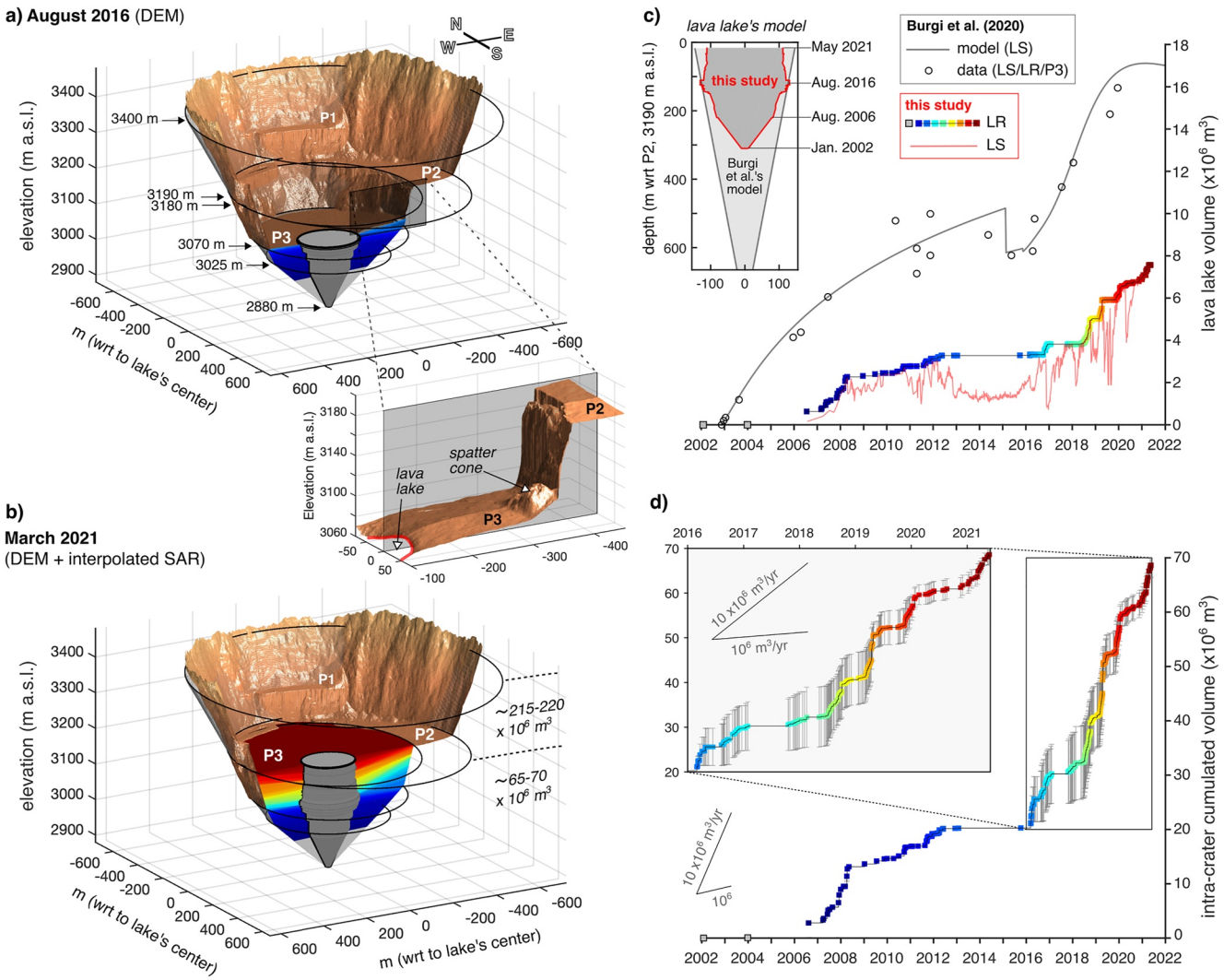

Figure 5. Evolution of Nyiragongo's crater between 2002 and 2021. (a) DEM cross-section from UAV-based photogrammetry model taken on August 8, 2016 (brown surface). The shape of the crater's bottom from 2,880 to 3,070 m a.s.l (*P3* altitude in 2016 DEM) is inferred from the photogrammetry result using IKONOS images on January 31, 2002 (see Section 3.1). Its filling by lava since the last eruption until August 2016 is illustrated by blue-to-red colors corresponding to estimates as plotted in time series in panels (c) and (d). (b) Same as in (a) with crater filling measures extended up to March 2021 following SAR data. (c) Lava lake volume (up to the lake's rim *LR* or to the lake's surface *LS*) for the period 2002–2021 according to the SAR-based measurements. Burgi et al.'s model and data (computed from supplementary code provided in Burgi et al., 2020, see Text S3 in Supporting Information S1) based on a simplified lava lake shape (inverted gray cone in inset) are plotted for comparison as a gray line and round markers, respectively. (d) Time series of the total intra-crater cumulated volume (including the lake). Error bars correspond to the uncertainty about the volume accumulated between the western and the eastern sides of the crater, which are large between 2016 and 2019 since only the highest section of the cone is illuminated on the eastern side.

the course of the years (e.g., Balagizi et al., 2016; Burgi et al., 2020; see also Figures 4 and S5 in Supporting Information S1). To consider a realistic evolution of the lava lake, we calculate its time-varying surface under the assumption of a permanent elliptical shape (e.g., Balagizi et al., 2016). To do so, we use, again, the amplitude information from SAR images, along the azimuth direction to avoid the layover effect. We directly convert pixels into meters using the azimuthal resolution of the sensor (see Text S1 and Table S1 in Supporting Information S1). Between 2006 and 2020, the N-S lake's width varies from ~140 to ~230 m and up to ~260 m along the E-W direction. Assuming the arrangement of five conical frustums as an accurate representation of the crater morphology (with bases located at 2,880, 3,025, 3,070, 3,180, and 3,190 m a.s.l., respectively; Figure 5a), we compute the volume of the lava lake (Figure 5c) and the total intra-crater extruded magma (Figure 5d).

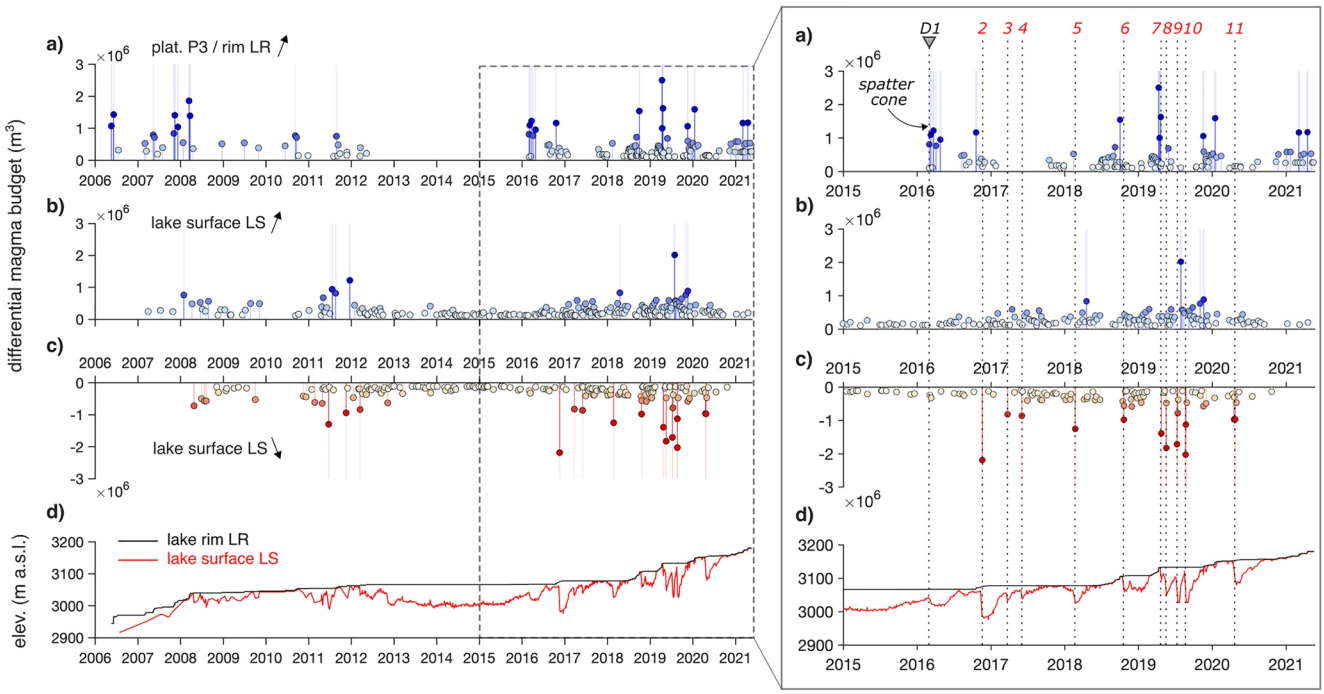

Figure 6. (a–c) Differential magma budget (i.e., between two successive measurements) inside Nyiragongo's crater calculated between May 19, 2006 and May 21, 2021 (on left) and zoomed in between January 1, 2015 and May 21, 2021 (on right). A positive magma budget (a, b) is due to either an increase of the platform *P3* and lake rim *LR* lave or an increase of the lake surface *LS*, respectively. A negative magma budget (c) only occurs during a drop of the lava lake level. Absolute differential magma budget lower than 0.1×10^6 m^3 are not plotted and values exceeding 0.75×10^6 m^3 are highlighted with shaded lines behind the corresponding markers. This allows to identify the main drops *D2–D11* on the right panel (2015–2021) (*D1* corresponds to the drop following the appearance of the spatter cone). (d) Absolute elevations of lava lake rim (*LR*) and lava lake surface (*LS*) as displayed in Figure 4.

In Figure 5c, SAR-based results show that the total volume of molten lava contained in the lake reached only ~0.63×10^6 m^3 between the January 2002 eruption and July 2006. The lava lake then evolved quickly during the 2 following years to contain up to ~2.3×10^6 m^3 in 2008. Over the next 8 years (2008–2016), the volume increased by only 1×10^6 m^3 and reached ~3.3×10^6 m^3. The appearance of the cone in early 2016 marks the beginning of several time-limited pressure increases, leading to an overall volume of ~7.5×10^6 m^3, which is the maximum estimate in May 2021 at full capacity (i.e., when the lava lake surface *LS* is at the level of the lava lake rim *LR*).

Similarly, we compute the first reliable time series of total volume of lava accumulated in the crater (including the lava lake) in the period 2002–2021 (Figure 5d). Taking into account the crater's conical shape, the amount of lava accumulated since the appearance of the cone in early 2016 is about 2.5 times greater than the volume accumulated between 2002 and 2016, that is, ~50×10^6 m^3 versus ~20×10^6 m^3, respectively. The alternating plateaus and pulsatory growths are obvious for the period 2016–2020. It is worth noting that the overall intra-crater accumulation rate observed since 2016 is similar to the 2006–2008 rate, that is, about 10×10^6 m^3/year. It should also be noted that the lava flows from the spatter cone inundating the platform *P2* on the Eastern side from mid-2020 until May 2021 (see Figure S5 in Supporting Information S1) cannot be retrieved because this amount of lava did not exceed one pixel at the illuminated point on the SAR image in slant range plane (i.e., point B in Figure 2b). A uniform inundation over an entire unified bottom platform (i.e., *P3* reaching *P2*) detected with a height resolution of about 1.8 m (Sentinel S1) would give an additional volume of around 1.3×10^6 m^3.

We compare here the lava-lake volumes with the ones from the last iteration of Burgi et al. (2020) model, which applied closed-system numerical simulations of magma flows and accumulation between the lava lake and the shallow magma chamber (e.g., Huppert & Hallworth, 2007). The set of 20 field estimates of *LR* and/or *P3* elevations coming from different sources used for constraining their model is also plotted. As stated earlier, a detailed discussion about these data and model is provided in the Supporting Information (Text S3, Figure S4, Tables S3–S4 in Supporting Information S1). The modeled extruded volumes agree qualitatively with the SAR-based

results, both showing an overall increase, but this remains the only common feature between the present results and the Burgi et al. (2020) model.

Assuming a deep inverted conical lava lake, which strongly differs from the shape derived here (Figure 5c, inset), Burgi et al. (2020) indicate that the lava lake's pit crater would contain a minimum of 16×10^6 m^3 of molten lava in 2020, which is more than two times the result derived from the SAR-based measurements (Figure 5c). We see no sign of an important discontinuity (i.e., a lava-lake-level drop) in 2015 as imposed in the Burgi et al. model. The underlying assumption behind this drop, though unconfirmed by field measurements as stated by the authors (see data points in Figure 5c), would be the depressurization of the shallow magma chamber related to the opening of a new dyke linking the shallow reservoir to the spatter cone appearing in early 2016 (see Section 3.6 for a different origin of this spatter cone supported by our results). Burgi et al.'s model also predict a decreasing extrusion rate and stabilization of the lave-lake level in the course of the years 2020–2021, which was not observed before the flank eruption in May 2021. Based on the data presented here, about 30×10^6 m^3 did accumulate within the crater between 2017 and 2020, which is 60% of the volume estimated by Burgi et al. (2020) (i.e., 50×10^6 m^3 after assuming a constant diameter of 800 m for *P3*).

3.4. Temporal Evolution of Intra-Crater Magma Budget

The filling of Nyiragongo's crater by fresh lava since 2002 was a discontinuous and pulsating process. Using information from the intra-crater volumes (Figure 5), we compute the temporal evolution of magma budget inside Nyiragongo's crater since the first SAR measurement in 2006 (Figure 6a–c). Positive budgets (increase of *P3*, *LR*, and/or *LS*) are colored in blue (Figures 6a and 6b), negative in red (decrease of *LS*, Figure 6c). The first positive budget value in Figure 6a (∼1 x 10^6 m^3) corresponds to the amount of lava accumulated between the renewal of lava lake activity in 2002 and the first SAR measurement on May 19, 2006. Nearly 3×10^6 m^3 accumulated into the crater two months later. For lava lake budget (Figures 6b and 6c), each value corresponds to a differential measurement between two successive SAR-based results with a median spacing of 4 days (the 95th percentile is 19 days since 2006 and 8 days since 2012). Only differential budgets above 0.1×10^6 m^3 are plotted. As observed in Figure 5, we can identify a nearly steady-state period of about 3 years in 2013–2015 between two phases of lava accumulation within the crater (2006–2012 and 2016–2021). Zooming into the last time period 2015–2021, we can easily identify 10 periods of marked and sudden lava lake drops between November 2016 and April 2020 (see red triangles numbered *D2* to *D11* in red in Figure 6), each of which has a negative magma budget lower than -0.75×10^6 m^3. Another clear, but lower drop preceding these 10 events initiated between February 28 and March 4, 2016 (see gray triangle *D1* in Figure 6) and is not associated with a significant negative magma budget. This event is most likely related to the birth of the spatter cone on the crater floor on February 29, 2016, as described by Balagizi et al. (2016) (see Section 3.6).

Plotting in Figure 6d, the daily interpolated evolution of the lava lake's surface and rim (*LS* and *LR*, respectively), as also done in Figure 4, helps to analyze the evolution of the differential (∼weekly) magma budget inside Nyiragongo's crater. For (sparser) data obtained before 2013, large drops occurred during a time period marked by an overall increase of the bottom platform (i.e., an overall positive magma budget). An increasing temporal resolution since 2015 allows for a better evaluation of this potential relation (i.e., positive magma budget and lake-level drops). Relying on Figure 6d, we can clearly see that large drops *D2–D11* are preceded in the months before either by an increase of the lava lake (positive magma budget in Figure 6b) and/or by an increase of the bottom platform (lake overflowing and/or spatter cone lava flows, positive magma budget in Figure 6a). Similarly, even if the daily magma budget did not evolve quickly, an overall continuous positive balance has been observed since mid-2015, a bit less than 1 year prior the appearance of the spatter cone in March 2016 and the synchronous lake drop (*D1*). Between 2013 and 2015, no significant drops of the lava-lake level occurred during a long-term quiescent period indicated by stable lava-lake level (∼50 m below the lake rim).

While explaining the positive magma budget within the crater by an overall overpressure in the magmatic system is straightforward, the origins of the sudden large lava lake drops remain less obvious based only on visual or surface observations. For instance, Bobrowski et al. (2017) suggested that a sudden ∼20–25 m lava lake drop visually observed in June 2011, which is also detected by the SAR-based measurement (Figure 4), was due to a pressure drop initiated by the displacement of gas. On another hand, Barrière et al. (2019) showed that the few seismic records available at that time (from a station located about 17 km away from the summit) contained

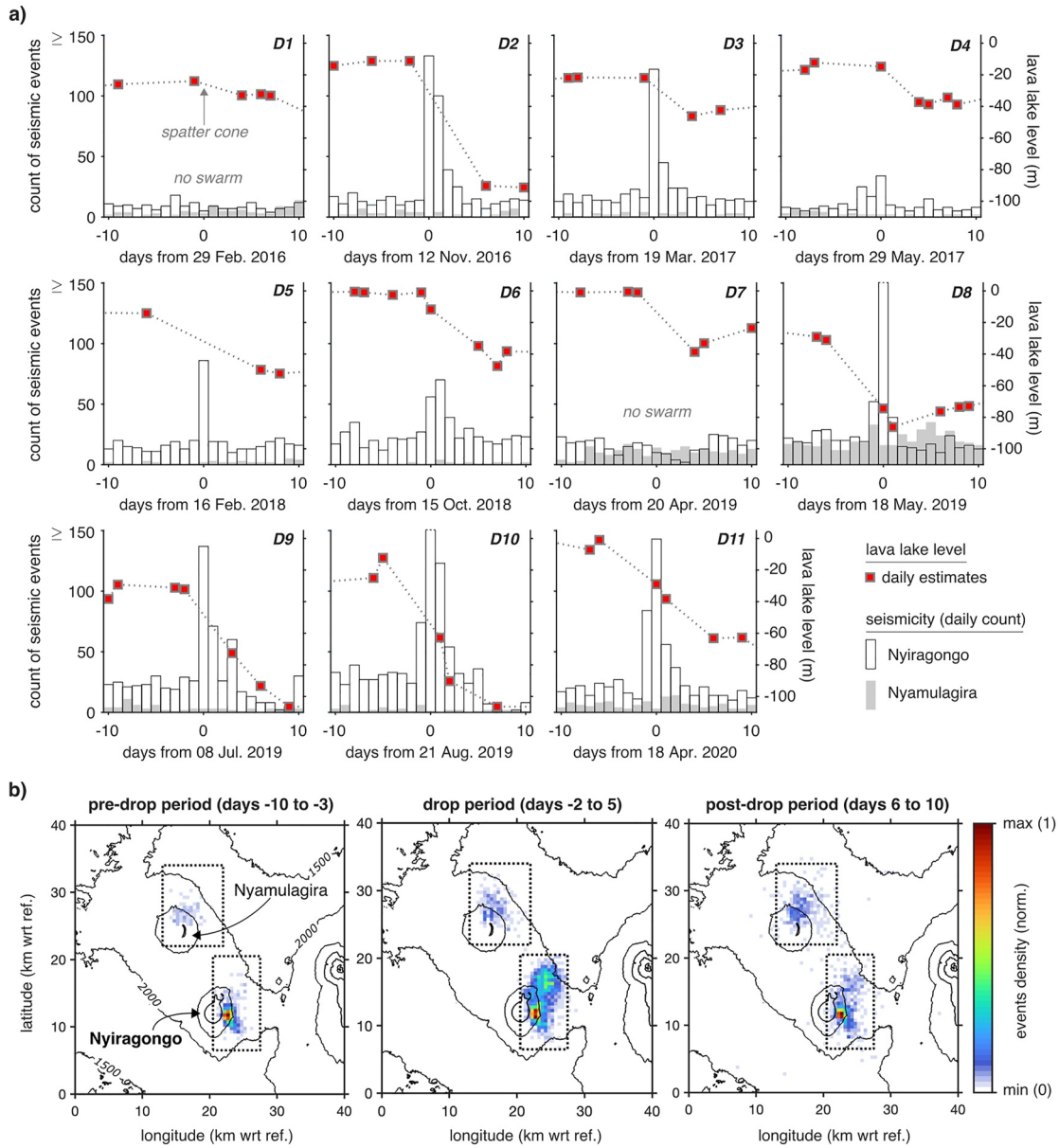

Figure 7. (a) Histograms of seismic events count at Nyiragongo (transparent bar) and Nyamulagira (gray bar) during ±10-day window around the drops *D1–D11* identified in Figure 6. SAR-based estimates of the lava lake's surface level from its rim (expressed in negative values, *LL* in eq. 3) for the corresponding periods are also plotted as red square markers. All subplots have the same axis scales. Count peaks for *D8* and *D10* exceed the maximum value of the left ordinate scale, which is set to 150 for visual purpose. (b) Normalized events density maps for pre-drop (days −10 to −3 in (a)), drop (days −2 to 5 in (a)), and post-drop periods (days 6–10 in (a)). Each map is obtained by stacking all events locations during the ±10-day windows *D1–D11*.

evidence of a seismic swarm synchronous with the lava lake drop, thus paving the way for explaining large decameter-scale drops of the lava lake level through magma movement at depth.

3.5. Focus on the Largest Lava Lake Drops and Their Seismic Signature

The appearance of a spatter cone next to the lava lake since March 2016 is a time marker of a new intra-crater eruptive sequence characterized by several large drops of the lava lake levels (*D1–D11* in Figure 6). Using seismic data from KivuSNet, Barrière et al. (2018, 2019) studied the detailed seismic signature (count, type of events, and location) of the November 12 and 13, 2016 major pressure drop (*D2*). They showed that a swarm

of events occurred at depths larger than 10 km during the first hours of the ~80 m lava lake drop. These seismic events are characterized by a broad frequency content between 0.5 and 10 Hz. They differ from shallow low frequency (<2 Hz) seismo-acoustic events also observed during and after that drop, which reflect the intense spattering activity of the lava lake. Such a deep swarm of events with complex waveforms and broad frequency content could convey (potentially mixed) source mechanisms from fluid movements (e.g., crack resonance) to more classical tectonic processes (i.e., brittle failure). Determining their individual source mechanisms, which often are not well constrained for volcanic signals (due to path effects, poor SNR, unknown velocity structure, sparse station distribution, etc.), remains beyond the scope of this paper. Our main purpose here is to determine whether or not each major drop of the lava-lake level at the surface is associated with a seismic swarm at depth, similar to the one that occurred in November 2016.

Figure 7a shows the count of seismic events automatically located in the VVP (see Section 2.3) during a ± 10-day time-window around each major drop highlighted in Figure 6 (drops *D1–D11*). We choose to plot events not only associated to Nyiragongo but also to its neighboring active volcano, Nyamulagira. The density of events (for a longitude/latitude grid spacing of 0.5×0.5 km^2) is plotted in Figure 7b. Three time periods are defined as pre-drop, drop, and post-drop periods within the ±10-day windows plotted in Figure 7a. Counts for Nyiragongo and Nyamulagira depicted in Figure 7a are thus obtained by compiling events located inside the rectangles drawn in dashed lines around each volcano. Depending on the variable station availability between 2016 and 2020, the SNR of the seismic records and the location errors introduced by the use of a 1D velocity model, the 2D (longitude/latitude) uncertainty of the final location solutions is about a few kilometers in the worst cases (see Text S2 in Supporting Information S1). The stacking of 6,873 epicenters in the VVP for the selected periods *D1–D11* (231 days in total) leads to the density maps of earthquakes plotted in Figure 7b. These maps highlight the main seismicity patterns before (2052 events), during (3,770 events) and after (1051 events) the drops of the lava lake while limiting the influence of single location errors.

The first drop *D1* is related to the appearance of the spatter cone on February 29, 2016 (Balagizi et al., 2016). At that time, no seismic swarm is detected at Nyiragongo (see next Section 3.6). In contrast, each of the following large drops *D2–D11* is associated with a seismic swarm, except *D7* in April 2019 (also specifically discussed later in Section 4.1). The intense seismic activity generally spreads over 3 days at the maximum. In addition to the first major drop *D2* in November 2016, seismic swarms and lava lake drops are more pronounced for the last four events in 2019 and 2020 but, overall, there is no obvious relationship between the number of detected seismic events and the amplitude of the lava lake level drops.

One can note that the number of seismic events detected at Nyamulagira is usually much lower than at Nyiragongo, except during two time windows, *D7* and *D8*. Nyamulagira is a highly active volcano characterized by frequent flank or summit eruptions, and such patterns of increased seismicity are not unusual at that volcano (e.g., Barrière et al., 2017). The larger occurrence of seismic events during these two windows slightly influences the density of events at this volcano between the pre-drop, drop, and post-drop sequences plotted in Figure 7b. However, there is no noticeable seismicity at Nyamulagira for the other selected periods, which in turn excludes a relationship between these 10 (+*D1*) major lava-lake drops at Nyiragongo and the seismic activity at Nyamulagira.

On the contrary, at Nyiragongo, the event density depicts a clear change between the three phases. Before and after the lava-lake drops, the dominant pattern is a cluster east of Nyiragongo's central crater beneath the edifice. This important seismic feature at Nyiragongo conveys a dominant, stable seismic source at large depth (~11–15 km b.s.l.) repeating every day (Barrière et al., 2019). This non-destructive source is observed continuously for each time window selected here. During the lava-lake-level drops at Nyiragongo, the seismicity rather clusters in an elongated pattern extending SW-NE starting from the edifice.

In Figure 8, we plot the hypocenters (longitude, latitude, and depth) of seismic events observed during the 11 time windows centered around the major drops highlighted in Figure 7, including the first one linked to the appearance of the spatter cone. These events are regrouped into five time clusters (February–March 2016, November 2016 to May 2017, February–October 2018, May–August 2019, and April 2020). Compared to events plotted in Figure 7 (counts and density maps), we focus here on the swarm episodes. Therefore, we apply an additional selection criterion in order to ensure keeping the best constrained automatic solutions around Nyiragongo (see Text S2 in Supporting Information S1). This new catalog reduces to 970 events over a total of 35 days. The observed swarm-like and repetitive seismicity is of low magnitude ($M_L < 2.5$), which is typical for volcanic environments. It occurs

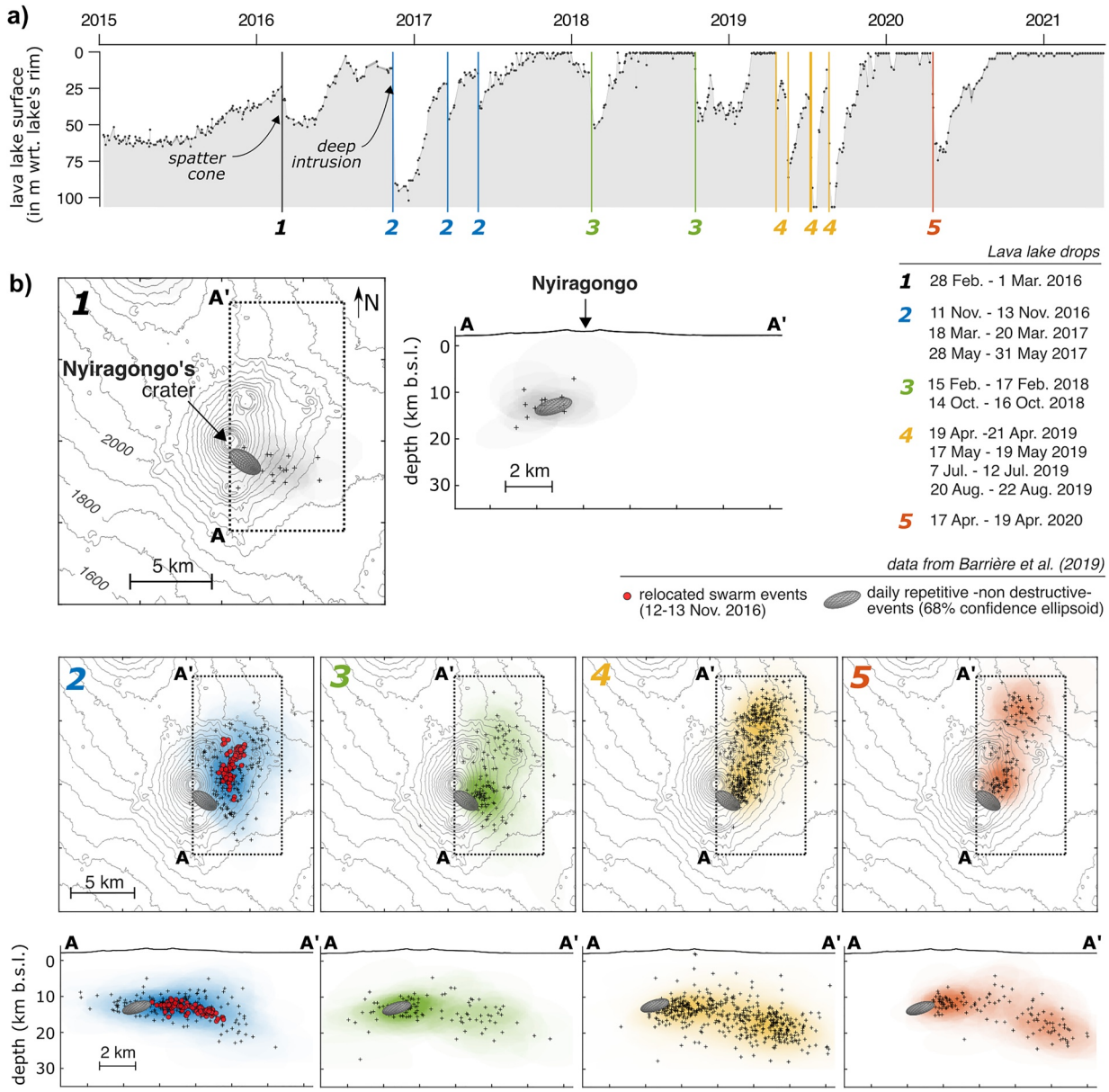

Figure 8. a) Lava lake surface disregarding the absolute elevation of the lava lake rim (i.e., *LR-LS*, the inverse of the lava-lake level *LL* (eq. 3) expressed in negative values in Figure 7). Five time clusters are selected from Figure 7 from which the corresponding seismic events locations are plotted in (b). (b) NS/EW location maps around Nyiragongo and depth sections of seismic events located within the dashed rectangle (projected on AA' profile) for time periods identified in (a) (exact dates are indicated at the right of the figure). The gray ellipsoid and the red dots (for the 2016–2017 period 2) correspond to the deep repetitive seismic source and the November 12 and 13, 2016 located in Barrière et al. (2019), respectively. The best hypocenter solutions of each individual seismic event are plotted as crosses and the associated colored shaded areas (2D projected ellipses) correspond to the location uncertainties (see Text S2 and Figure S3 in Supporting Information S1). The color becomes more pronounced when several events are located in a similar source area since all location ellipses are stacked.

mostly at a depth ranging between 10 and 20 km, which is in agreement with a former seismological investigation (Tanaka, 1983) and the deep storage zone inferred from petrological analyses (Demant et al., 1994). As previously mentioned, Barrière et al. (2019) already relocated the November 2016 seismic swarm using coupled master event (e.g., Evernden, 1969) and double-difference (Waldhauser & Ellsworth, 2000) location techniques (see Figure S1 in Supporting Information S1). We confirmed that the automatic locations of the November 2016 swarm give consistent results with the refined hypocenter solutions in Barrière et al. (2019) (red dots in Figure 8b). Some variability can be due to the evolving network layout (e.g., additional station deployments) between 2016 and 2020, but the chosen selection criteria should mitigate this effect. For instance, the few events

automatically located in cluster no. 1 (February 28 to March 1, 2016) would actually correspond to the repetitive seismic source relocated in Barrière et al. (2019) which is depicted as the 68% confidence ellipsoid in Figure 8b. Despite relatively large total location uncertainties (median values are 3.5 km in longitude/latitude and 9.8 km in depth), the SW-NE and deep seismicity pattern first observed in November 2016 repeated at each lava lake drop.

3.6. The Formation of the 2016 Spatter Cone

As evoked previously, a moderate though clear drop of the lava lake level of ~20 m occurs synchronously with the appearance of the spatter cone in late February/early March 2016 without significant seismic activity detected across the local network (*D1* in Figures 6–8). This suggests a direct hydraulic connectivity between the cone and the lake, in contradiction with a vent formation decorrelated from the lava lake level variations as stated by Burgi et al. (2018) and Pouclet and Bram (2021).

The higher elevation of the spatter cone with respect to the lava lake's surface, in conflict with hydrostatic equilibrium if both were connected, can be explained by a density-driven mechanism: The density of the hot, gas-rich lava rising through a narrow conduit branched from the lake's bottom up to the cone is lower than the overall molten lava contained in the lake, which is partly cooled and degassed. Neglecting additional dynamic pressure and temperature effects, a simple derivation from hydrostatic pressure formula at this bottom level would lead to:

$$h_C = \left[h_L \times \Delta_\rho\right] / \rho_C \tag{4}$$

where h_C is the height of the cone relative to h_L, the depth of the lake, ρ_C is the average density of lava inside the cone's conduit, and Δ_ρ is the positive density contrast between lake and cone lavas.

From available SAR-based results (Figure 4, see also Text S4 and Figure S6 in Supporting Information S1) and field observations (e.g., Burgi et al., 2018, 2020), the total cone's height ranges mostly between 20 and 60 m (and never exceeded 70 m). The cone height is shaped by fountaining-style eruptive activity where gas-rich lava jets, as observed in the field (e.g., lava fountains of about 5–20 m high observed by Burgi et al., 2018) could reach heights up to 50 m (e.g., La Spina et al., 2021). The main lava extrusion points feeding lava flows from the cone to the lake do not correspond to the uppermost altitude of the cone but are actually located closer to its base (Figure S7 in Supporting Information S1). Based on field observations in February 2020, Burgi et al. (2020) estimated a cone height of about 45–50 m and a slope of 7° for a lava tunnel of about 180-m length between the base of the cone and the eastern side of the lake rim (*LR*; see also Figure 5a for visualizing the lake-cone distance). This implies a differential height of about 20–25 m between the lava extrusion point at the base of the cone and the lava lake's rim.

In order to estimate the density of the ascending fresh lava ρ_C inside the cone's conduit, one has to take into account the important effect on density of bubble content. Indeed, density measurements of remelted rock samples (i.e., without any gas and crystal) lead to a value of 2,833 kg.m^{-3} at Nyiragongo (Morrison et al., 2020). However, the estimates of lava-lake density by Carbone et al. (2013) using gravity data at Kīlauea suggest a very low density of 950 ± 300 kg.m^{-3}, which indicates a very high gas content in the upper 100 m of that lake system. Therefore, if we also reasonably consider both lake and cone lava densities at Nyiragongo to be around 1,000 kg.m^{-3}, a density contrast of ~250 kg.m^{-3} would be enough to explain a height h_C up to about 75 m (i.e., differential height between the lava extrusion point at the base of the cone and the lava lake's surface). One should also note that the main growing stages of the spatter cone are associated with high lava lake levels, which indicates that the cone and the lake evolve simultaneously in response to a deeper pressure buildup and that a low differential height h_C is maintained (Text S4 and Figure S6 in Supporting Information S1). Hence, the density contrast between the lake and the cone's conduit might be smaller than expected to allow lava escaping from the cone (i.e., <100 kg.m^{-3}). The hypothesis of a spatter cone of a common shallow origin with the lake and shaped by a lower (gas-rich) lava's density appears therefore strengthened.

Instead, Burgi et al. (2018) suggested a deep source for the cone's lava through the fracturing of the rock over several km (>4 km) from the shallow reservoir to the summit, without connection to the existing nearby open conduit of the lava lake. However, according to Balagizi (2016), neither soil temperature nor CO_2 degassing measurements would support a magmatic intrusion from deep levels. Furthermore, the authors assume an overpressure larger than 10 MPa for supporting this dyke intrusion scenario, which would logically result in

significant seismicity (e.g., Bakker et al., 2016). This value exceeds the upper bound of the stress range inferred by Wauthier et al. (2012) from InSAR analysis for the opening of deep and shallow eruptive dykes in 2002, which were associated with noticeable seismicity detected by then only two analog seismographs in the VVP (Kavotha et al., 2002). However, there is no clear seismic pattern before, during, or after the appearance of the 2016 spatter cone (Figures 7 and 8). In particular, the closest stations (<25 km) did not exhibit any specific signals on February 29, 2016 at 01:00 a.m. UTC, which is the date associated to the opening of the cone according to Balagizi et al. (2016), who mention, however, a seismic signal that we cannot trace back (Figure S8 in Supporting Information S1). The timing of this new vent opening is thus mainly based on the testimony of rumbling and explosions (without felt earthquakes) by Virunga National Park guards posted close to Nyiragongo's rim during that night. Finally, it should be noted that a pre-existing ring of fissures in the crater floor was observed from 2012 to 2015 while the lava lake stayed at low level (Balagizi et al., 2016, see also Figure S5 in Supporting Information S1). This fracturing during a quiescent period of stable lava-lake level supports the role of subsidence (Smets, 2016) and thermal contraction (e.g., Browning et al., 2016) for explaining the shallow cracking of the lava rock formation inside the crater before the appearance of the spatter cone.

4. Discussion

4.1. A Years-Long Deep Dyke Intrusion Beneath Nyiragongo

One of the main findings previously highlighted is that each of the 11 main drops of the lava lake level (*D1–D11*) between 2016 and 2020 is generally preceded by a significant positive magma budget (Section 3.4), and this observation is also true for the period 2006–2012 (Figure 6). All drops (*D2–D11*) are associated with a clear crater filling (*2, 6, 7, 11*—Figure 6a) or a clear increase of the lava lake level (*1, 3, 4, 8, 9, 10*—Figure 6b) in the weeks/months before the drops. Although less obvious, even the drop *D5* is preceded by a small filling of the inner crater (Figure 6a), which actually occurs during a decreasing trend of the lake level (Figure 6d). The first drop *D1* is a peculiar case. Linked to the spatter cone formation, it is most likely a response to a long-term pressure buildup highlighted by the continuous rise of the lava lake initiated almost 1 year before in 2015. This behavior strongly suggests that surface manifestations (large drops of the lava lake level, appearance of the spatter cone) preceded by significant positive magma budget are connected by a causal mechanism. The intra-crater magma budget inferred from space-based SAR measurements could thus be considered a proxy for overpressure in the magmatic system.

However, we cannot define any systematic pattern of duration/amount of positive magma budget before each drop. For instance, in April 2020, a relatively quiescent period of at least 1 month preceded the lava lake drop. These overpressure regimes are obvious when the lava reaches the lake rim and accumulates within the crater by inundating *P3* and/or during episodes of spatter cone activity (lava fountaining, lava flows; see Figure 6a). These periods of marked overpressure are noticeable in late 2018 and in the course of the year 2019. The first drop in November 2016 is also preceded by noticeable effusive activity from the spatter cone (see Figure S7 in Supporting Information S1), even though to a lesser extent than the ones leading to major extruded volumes between 2018 and 2020. Less obvious overpressures in the plumbing system are also detectable thanks to the monitoring of the lava lake level. Following the 2016 initial drop, two successive lava lake drops occurred in 2017 during the progressive rising limb of the lava lake level. In these cases, there was no clear surface manifestation (i.e., no lake overflowing, no cone effusive activity).

Here, we notice that the seismic swarm events spread over a continuously enlarging area from Nyiragongo since the first drop in November 2016 and depict a clear progression toward the NE direction until 2020. A rough estimate of the maximum extent of these successive swarm episodes would be up to about 10 km. Hence, we show that the origins of the main pressure drops between 2016 and 2020 lie in several successive deep magmatic intrusions occurring along a path that shares the orientation of the principal rift faults of the Precambrian basement in the VVP (Smets, 2016), leading each time to a partial siphoning of the lava lake system. Only one period out of the 10 major drops does not exhibit a clear synchronous seismic swarm, that is *D7* in April 2019. As the seismic network has been continuously operational since late 2015, we suggest that this specific intrusion period behaved more aseismically than others because, at such large depth, the dyke could cool over periods of months and remain open between successive phases of progression (e.g., Buck et al., 2006).

As already pointed out by Barrière et al. (2018) in their study of the November 2016 drop (*D2* in this study), such a swarm-drop relation was also observed at Kīlauea (Halema'uma'u crater) by Patrick et al. (2015). Between 2010 and 2011, inflation episodes measured by GPS and tilt stations at Kīlauea's summit were accompanied by seismic swarms and a rise in lake levels. These clear observations indicated an increase of the pressure within the magmatic system before three large lava lake drops (~200 m for the largest), which were all associated with eruptive events on the East Rift Zone (ERZ). Relatively small short-term precursors from the same type of observations (deformation, lava-lake level) were observed before the 2018 eruption and the draining of the Halema'uma'u lava lake. This major intrusive and eruptive event was also preceded by an increase of earthquake rates commonly linked to summit pressurization (<5 km b.s.l.; Patrick et al., 2020). In contrast, Barrière et al. (2018, 2019) noted that the deep seismic swarm at Nyiragongo on November 12 and 13, 2016 was synchronous, not precursory, to the drop of the lava-lake level (see also Figure S1 in Supporting Information S1). This implies a very efficient hydraulic connectivity between the shallow and deep parts of the magmatic system at Nyiragongo. We confirm here the same synchronicity between lava-lake-level drops and seismic swarms during the major episodes between 2016 and 2020. In absence of precursory seismicity and without long-term high-resolution ground deformation measurements at the summit of Nyiragongo (as available at Kīlauea), Barrière et al. (2018) pointed out the difficulty with inferring any signs of pressurization before the November 2016 drop.

The continuous time series of crater topography changes and lava-lake-level variations derived here from SAR measurements are the first evidence of repetitive pulsatory pressure buildup sequences at Nyiragongo, followed by deep magmatic intrusions along the same path and associated with sudden drops of its lava-lake level. It is also worth noting that the major lava-lake-level drops between 2016 and 2020 occur at progressively higher altitudes with time (Figures 4b, 5c, and 6d). The pressure increases in the magmatic system cause the level rise until the pressure becomes large enough to initiate a magmatic intrusion at depth. The longer the dyke, the higher must be the breakout pressure to initiate the next step. Although the pressure started rising slowly a few months prior the 2021 eruption, as it did for instance at the end of 2019-beginning of 2020 (see magma budget in Figure 6a), the May 2021 eruption started without such a deep swarm. This means that this flank eruption was not associated with one of these deep intrusions below the edifice (Smittarello et al., 2021).

4.2. Toward a Deeper Understanding of Nyiragongo's Plumbing System

Like most volcanoes, Nyiragongo's plumbing system is poorly constrained. As shown in the present study, its open-vent crater and persistent eruptive activity is nonetheless a remarkable source of information to understand magmatic pressure changes. The combined use of seismicity and lava-lake-level allows us to infer a remarkable connectivity between the shallow lava-lake system and the deep plumbing system (>10 km b.s.l.) since the lava-lake level reacts synchronously with deep magmatic intrusions. However, open systems do not favor ground inflation due to a limited pressurization in the shallowest part of the magma plumbing system (e.g., Chaussard et al., 2013). Compared to closed volcanic systems, this is a drawback to inverting ground deformation for estimating source parameters, yet this remains a prerequisite for investigations of magma storage volumes and supply rates (beyond other exploratory approaches, for example, using thermal and SO_2 monitoring data from space as done by Coppola et al., 2019). However, at Kīlauea, repetitive deflation-inflation (DI) events lasting for hours to days were reported for decades without leading to eruptive events or intrusions in the ERZ or at the summit (Anderson et al., 2015), notably since 2008 through the observation of decameter-scale rises and drops of the Halema'uma'u lava lake (Patrick et al., 2019). These numerous short-lived events desynchronized from eruptive events are associated with transient pressurization of a shallow magma reservoir (Anderson et al., 2015). Based on high-temporal-resolution tilt and lava-lake-level measurements during one of these large DI events, Anderson et al. (2015) obtained a reservoir volume of about 1 km^3 (0.2–5.5 km^3 at 95% confidence) while Anderson et al. (2019) estimated the volume of magma stored before the May 2018 eruption to 2.5–7.2 km^3 (at 68% confidence) using high-quality multiparameters geodetic observations (tilt, GPS, and InSAR interferograms).

Based on sparse lava-lake elevation measurements (20 data points in ~18 years, see Figure 5c), the simulations proposed by Burgi et al. (2014, 2018, 2020) are the first attempts for estimating intruded volumes after assuming a simplified geometry, that is, a vertical cylindrical conduit (4 km long, diameter of 15 m) linking a conical lava lake to a shallow magma chamber. They explained the continuous surface activity at Nyiragongo from the convective magma movement controlled by density and viscosity differences between the gas-rich ascending

magma and the descending cooled and degassed magma (e.g., Stevenson & Blake, 1998). The diameter value of 15 m was chosen to be representative of basaltic volcanoes and should explain the visual testimony of a lava lake drop of ~25 m occurring in less than 1 min on June 3, 2011 (Burgi et al., 2014). For the same drop event, Bobrowski et al. (2017) indicated a timing of seconds to minutes and fixed an upper limit of 5 min. According to fluid-flow equations applied by Burgi et al. (2014), such timing variability implies, however, a very large error margin around the choice of 15 m (the diameter of the conduit could be two times or half this value as well). To date, measurements at the summit with high accuracy and temporal resolution are still needed to better constrain such an estimate. According to the physical framework applied by Burgi et al. (2014), the conduit's length has a minor effect on the modeled magma supply rate compared to the conduit's diameter. However, the chosen depth for the magma chamber roof (i.e., 1–4 km) should have a strong influence on deformation expected at the surface, which was not considered in this set of studies. In line with extruded volumes as predicted by their model (see Figure 5c), Burgi et al. (2018) suggested a ~10 km^3 spheroidal shallow reservoir (6 km long and 0.6 km high) beneath the volcano, and mentioned an intruded volume of 0.9 km^3 in 2018. Burgi et al. (2020) forecast (before the occurrence of the May 2021 eruption) a 2 km^3 intruded volume in 2025.

Qualitative information about the influence of a deformation source at shallow depth can be obtained using a point source model (Beauducel, 2019). We acknowledge that this approach is too simplistic and could encompass large uncertainties. Nonetheless, during short inflationary/deflationary episodes linked to Halema'uma'u lake level variations, a point source model proved a useful approach for interpreting tilt measurement related to volume variations in the shallow magma chamber of Kīlauea (Anderson et al., 2015). At Nyiragongo, a volume dilatation of 1 km^3 at 4 km depth (approx. the lower bound of intruded volume predicted by Burgi et al. models) would produce vertical displacements from about 0.1 to 15 m within a distance of 20 km around the edifice (see Figure S9 in Supporting Information S1). Using measurements between 2009 and 2016 from the continuous GNSS monitoring network KivuGNet in the VVP, Geirsson et al. (2017) showed that the main surface deformations are associated with the eruptive activity of the large Nyamulagira shield volcano (only ~14 km northwest of Nyiragongo). Inter-eruptive deformations (with respect to Nyamulagira's activity) never exceeded a few centimeters and could be associated with magma accumulation under the Nyamulagira-Nyiragongo volcanic system. To date, preliminary investigations of available InSAR and GNSS observations (e.g., Geirsson et al., 2019) do not suggest any long-term significant inflation of Nyiragongo's edifice or short-term DI episodes of the shallow magma chamber linked to lava-lake-level variations. Applying a point source model to Villarica lava-lake volcano, Witter et al. (2004) suggested endogenous growth deeper than the shallow volcanic edifice to explain the imbalance between extruded and intruded volumes without significant surface deformation, as proposed for other persistently active volcanoes (e.g., Allard, 1997; Francis et al., 1993).

A more detailed investigation of these questions remains beyond the scope of this article and will be the subject of future dedicated studies. For instance, in the absence of continuous summit deformation measurements at Nyiragongo, the use of seismic ambient noise interferometry for monitoring seismic velocity changes beneath the edifice, such as done by Donaldson et al. (2017) at Kīlauea, could be a promising tool to detect potential signs of short- and long-term (de-)pressurization with high temporal resolution within the shallow plumbing system at Nyiragongo. It is also clear at this point that a deeper understanding of magma supply and storage at such a persistently active open-vent volcano would strongly benefit from the analysis of the first ever well-monitored flank eruption at Nyiragongo in May 2021 (e.g., Global Volcanism Program, 2021) while integrating other multi-parameter observations beyond crater topography changes only, such as InSAR, GNSS, SO_2 degassing, thermal anomalies, and seismic measurements.

Conclusions and Perspectives: What Does the Amount of Extruded Lava Could Tell Us About the Level of Unrest at Nyiragongo ?

The SAR-based method SAsha detailed in this article allows us to obtain the first decades-long time series of accurate lava-lake level and accumulated volume within the crater of Nyiragongo. Incremental lava accumulation within Nyiragongo's crater obviously indicates a sustained internal pressure of the magmatic system. A key observation is that the bottom platform *P3* prior the 2021 eruption was as high as before the 2002 flank eruption.

While periods of significant magma supply (e.g., 2007) have alternated with nearly steady-state conditions (e.g., 2014), a noticeable change in eruption dynamics has been observed since 2016. This change was characterized

at the surface by the appearance of a spatter cone and multiple, time-limited supply events of fresh magma accumulating within the crater. In the present study, we show that the largest drops of the lava-lake level were often preceded by noticeable pulsatory increases of extrusion rate and are accompanied, but not preceded, by significant seismicity. The combination of seismic observations with SAR-based lava lake level measurements allows us to infer the magmatic processes behind these repetitive patterns as multiple failures occurred at large depths (>10 km b.s.l) between 2016 and 2020 (and most likely before, e.g., in June 2011). There is no clear precursory signal to such deep failure that is detectable from surface observations, but it is remarkable that observing changes in extrusion rate within the crater provides clues on the changing stress conditions before and after the intrusions.

The absence of noticeable seismicity during the appearance of the 2016 eruptive cone, which is correlated with a drop of the lava-lake level, indicates that the spatter cone is most likely shallowly connected to the lava lake. This interpretation only requires the assumption of a reasonable density contrast between the lava lake and the lava feeding the cone and explains the simultaneous response of the cone eruptive activity and lava-lake level to deeper pressure drop or build up. Although being of shallow origin, its appearance was a clear marker of a change in summit eruption dynamics initiated since mid-2015 and stopped by the flank failure in May 2021.

The last months studied here (November 2020 to May 2021) experienced a renewal of lava flows from the cone and/or lake overflows inundating the bottom platform. As inferred from the analysis of the 2016–2020 time period, a new lava lake drop could have happened anytime in response to this pressure buildup, provided that the overpressure would have reached the required value to initiate the intrusion, which is increasing in time as we have shown. On May 22, 2021, magma movements did not follow the deep intrusion path at large depth as observed in the past years. Instead, magma flowed through the fractured top of the edifice toward the surface, leading to the drainage of the superficial lava lake system and the partial collapse of the inner crater (roughly along the separation between the former platforms *P2* and *P3*). Intermittent lava-lake activity reappeared inside Nyiragongo's crater about 4 months after this May 2021 eruption (GVO's personal communication and Georiska [2021]).

As observed for the 2002 and 2021 eruptions, the timing of such failures does not obey a simple level/pressure threshold. At Nyiragongo, the sole use of lava lake and/or platform elevation as time marker for forecasting a future eruption would indeed put aside the drastically different pre-eruptive states of the volcano. During about 6 years before the 2002 eruption, a cooled platform and encrusted lava lake were at steady altitude around 3,185 m a.s.l, which was not the case before the 2021 eruption. Moreover, the notion of maximum height of lava conveying a critical pressure equilibrium (e.g., Pouclet & Bram, 2021) is ambiguous since a 1977 critical setting exceeds by far the 2002/2021 threshold (see Figure 1b). While the 2002 eruptive sequence was most likely triggered by a regional rifting event (e.g., Komorowski et al., 2002; Wauthier et al., 2012, 2015), the 2021 eruption seems both controlled by sustained magmastatic pressure and a structural weakness resulting from the 2002 eruption (Smittarello et al., 2021). In the different geological contexts of Hawaii, similar conclusions were drawn by Patrick et al. (2019) when comparing old (1910–1930) and more recent (2008–2018) level variations of the Halema'uma'u lava lake before each eruption. High or rapidly rising levels of the lava lake confirmed a posteriori the greater chance to get a rift zone eruption but, as highlighted by the 2018 eruption at Kīlauea, the detection of a possibly impending eruption cannot rely on the unique use of such observations after defining a static level threshold.

In addition to such valuable information derived from changes of the crater topography and variations of the lava-lake level, the joint analysis of spatially and temporally dense ground- and space-based data (seismicity, deformation, degassing, etc.) remains essential for a better understanding of the intracrateral eruptive pattern, especially for a volcanic system like Nyiragongo with limited historical data. From that perspective, this study provides fundamental insights into Nyiragongo intra-crater eruptive behavior and origins from one flank eruption to another, of which trigger mechanisms must be specifically addressed in further investigations.

Data Availability Statement

B. Smets bought the couple of IKONOS images (DigitalGlobe). The authors are grateful to ESA for providing the Sentinel-1 and ENVISAT products for free, to Belspo and the Virunga Supersite Initiative for funding COSMO-SkyMed images (Italian Space Agency) and to Natural Resources Canada (NRCan) for sharing RADARSAT-2

images (Canadian Space Agency). Seismic data archiving and accessibility are ensured through the GEOFON program of the GFZ German Research Centre for Geosciences (http://dx.doi.org/doi:10.14470/XI058335) and KivuSNet is registered within the FDSN with network code KV (http://www.fdsn.org/networks/detail/KV/). All time series and seismic catalogs presented here are available as Supporting Information.

Acknowledgments
This article results from the sum of several contributions obtained in the framework of past and ongoing research projects funded by the STEREO-III Programme of the Belgian Science Policy Office (Belspo), and the Fonds National de la Recherche (FNR) of Luxembourg. These projects include RESIST (Contract SR/00/305), MUZUBI (Contract SR/00/324), and VeRSUS (Contract SR/00/382). The authors are grateful to ESA, Belspo, the Virunga Supersite Initiative, and Natural Resources Canada (NRCan) for providing satellites images (see Data Availability Statement). The authors thank the entire team of the Goma Volcano Observatory and the sentinels of the monitoring stations, without whom the operation of KivuSNet would be impossible. The authors also thank Halldór Geirsson (University of Iceland), Sergey Samsonov (NRCan), and Katcho Karume (GVO) for former collaboration on this work, as well as the Congolese Institute for Nature Preservation (ICCN) and the MONUSCO (UN stabilization mission in Congo) for their continuous support, including hosting seismic stations in their compounds. The SAsha method benefits from the Mex/C-code written by Tom Goldstein (Univ. Maryland) implementing the Split-Bregman algorithm (https://www.ece.rice.edu/ltag7/Tom_Goldstein/Split_Bregman.html, last accessed 24 February 2022). The authors would like to thank the reviewers J. Suckale and M. Patrick and the editor M. Poland for their constructive comments and suggestions that have helped us improve the original manuscript.

References

Agisoft, LLC. (2020). *Agisoft Metashape user manual*. Professional Edition.Version 1.6.

Allard, P. (1997). Endogenous magma degassing and storage at Mount Etna. *Geophysical Research Letters*, *24*(17), 2219–2222. https://doi.org/10.1029/97gl02101

Anderson, K. R., Johanson, I. A., Patrick, M. R., Gu, M., Segall, P., Poland, M. P., et al. (2019). Magma reservoir failure and the onset of caldera collapse at Kīlauea Volcano in 2018. *Science*, *366*(6470). https://doi.org/10.1126/science.aaz1822

Anderson, K. R., Poland, M. P., Johnson, J. H., & Miklius, A. (2015). Episodic deflation-inflation events at Kīlauea Volcano and implications for the shallow magma system: Chapter 11. In R.Carey, V.Cayol, M. P.Poland, & D.Weis (Eds.), *Hawaiian volcanoes: From source to surface* (Vol. 208, pp. 229–250). Washington, D.C. American Geophysical Union; John Wiley & Sons. https://doi.org/10.1002/9781118872079.ch11

Bakker, R. R., Fazio, M., Benson, P. M., Hess, K., & Dingwell, D. B. (2016). The propagation and seismicity of dyke injection, new experimental evidence. *Geophysical Research Letters*, *43*, 1876–1883. https://doi.org/10.1002/2015gl066852

Balagizi, C. M., Yalire, M. M., Ciraba, H. M., Kajeje, V. B., Minani, A. S., Kinja, A. B., & Kasereka, M. M. (2016). Soil temperature and CO2 degassing, SO2 fluxes and field observations before and after the February 29, 2016 new vent inside Nyiragongo crater. *Bulletin of Volcanology*, *78*(9), 1–11. https://doi.org/10.1007/s00445-016-1055-y

Barrière, J., d'Oreye, N., Oth, A., Theys, N., Mashagiro, N., Subira, J., et al. (2019). Seismicity and outgassing dynamics of Nyiragongo volcano. *Earth and Planetary Science Letters*, *528*. https://doi.org/10.1016/j.epsl.2019.115821

Barrière, J., d'Oreye, N., Oth, A., Geirsson, H., Mashagiro, N., Johnson, J. B., et al. (2018). Single-station seismo-acoustic monitoring of Nyiragongo' s lava lake activity, D.R. Congo. *Frontiers of Earth Science*, *6*. https://doi.org/10.3389/feart.2018.00082

Barrière, J., Oth, A., Theys, N., d'Oreye, N., & Kervyn, F. (2017). Long-term monitoring of long-period seismicity and space-based SO2 observations at African lava lake volcanoes Nyiragongo and Nyamulagira (DR Congo). *Geophysical Research Letters*, *44*(12), 6020–6029. https://doi.org/10.1002/2017GL073348

Beauducel, F. (2019). Mogi: Point source of dilatation in elastic half-space. MATLAB central file exchange. Retrieved from https://www.mathworks.com/matlabcentral/fileexchange/25943-mogi-point-source-of-dilatation-in-elastic-half-space

Bobrowski, N., Giuffrida, G. B., Yalire, M., Lübcke, P., Arellano, S., Balagizi, C., et al. (2017). Multi-component gas emission measurements of the active lava lake of Nyiragongo, DR Congo. *Journal of African Earth Sciences*, *134*, 856–865. https://doi.org/10.1016/j.jafrearsci.2016.07.010

Browning, J., Meredith, P., & Gudmundsson, A. (2016). Cooling-dominated cracking in thermally stressed volcanic rocks. *Geophysical Research Letters*, *43*(16), 8417–8425. https://doi.org/10.1002/2016GL070532

Brunner, D., Lemoine, G., Bruzzone, L., & Greidanus, H. (2010). Building height retrieval from VHR SAR imagery based on an iterative simulation and matching technique. *IEEE Transactions on Geoscience and Remote Sensing*, *48*(3), 1487–1504. https://doi.org/10.1109/TGRS.2009.2031910

Buck, W. R., Einarsson, P., & Brandsdóttir, B. (2006). Tectonic stress and magma chamber size as controls on dike propagation: Constraints from the 1975–1984 Krafla rifting episode. *Journal of Geophysical Research: Solid Earth*, *111*(B12). https://doi.org/10.1029/2005JB003879

Burgi, P.-Y., Boudoire, G., Rufino, F., Karume, K., & Tedesco, D. (2020). Recent activity of Nyiragongo (Democratic Republic of Congo): New insights from field observations and numerical modeling. *Geophysical Research Letters*, *47*(17), 1–11. https://doi.org/10.1029/2020GL088484

Burgi, P.-Y., Darrah, T. H., Tedesco, D., & Eymold, W. K. (2014). Dynamics of the Mount Nyiragongo Lava Lake. *Journal of Geophysical Research: Solid Earth*, *119*, 4106–4122. https://doi.org/10.1002/2013JB010895

Burgi, P.-Y., Minissale, S., Melluso, L., Mahinda, C. K., Cuoco, E., & Tedesco, D. (2018). Models of the formation of the 29 February 2016 new spatter cone inside Mount Nyiragongo. *Journal of Geophysical Research: Solid Earth*, *123*(11), 9469–9485. https://doi.org/10.1029/2018JB015927

Carbone, D., Poland, M. P., Patrick, M. R., & Orr, T. R. (2013). Continuous gravity measurements reveal a low-density lava lake at Kīlauea Volcano, Hawai'i. *Earth and Planetary Science Letters*, *376*, 178–185. https://doi.org/10.1016/j.epsl.2013.06.024

Chaussard, E., Amelung, F., & Aoki, Y. (2013). Characterization of open and closed volcanic systems in Indonesia and Mexico using InSAR time series. *Journal of Geophysical Research: Solid Earth*, *118*(8), 3957–3969. https://doi.org/10.1002/jgrb.50288

Coppola, D., Laiolo, M., Massimetti, F., & Cigolini, C. (2019). Monitoring endogenous growth of open-vent volcanoes by balancing thermal and SO2 emissions data derived from space. *Scientific Reports*, *9*(1), 1–12. https://doi.org/10.1038/s41598-019-45753-4

Demant, A., Lestrade, P., Lubala, R. T., Kampunzu, A. B., & Durieux, J. (1994). Volcanological and petrological evolution of Nyiragongo volcano, Virunga volcanic field, Zaire. *Bulletin of Volcanology*, *56*(1), 47–61. https://doi.org/10.1007/BF00279728

Derauw, D., Nicolas, d'.O., Jaspard, M., Caselli, A., & Samsonov, S. (2020). Ongoing automated ground deformation monitoring of Domuyo - Laguna del Maule area (Argentina) using Sentinel-1 MSBAS time series: Methodology description and first observations for the period 2015–2020. *Journal of South American Earth Sciences*, *104*, 102850. https://doi.org/10.1016/j.jsames.2020.102850

Donaldson, C., Caudron, C., Green, R. G., Thelen, W. A., & White, R. S. (2017). Relative seismic velocity variations correlate with deformation at Kīlauea volcano. *Science Advances*, *3*(6). https://doi.org/10.1126/sciadv.1700219

d'Oreye, N., Derauw, D., Samsonov, S., Jaspard, M., & Smittarello, D. (2021). MasTer: A full automatic multi-satellite InSAR mass processing tool for rapid incremental 2D ground deformation time series. *Paper presented at the 2021 IEEE international geoscience and remote sensing symposium (IGARSS)* (pp. 1899–1902). https://doi.org/10.1109/IGARSS47720.2021.9553615

Durieux, J. (2002). Volcano Nyiragongo (D.R. Congo): Evolution of the crater lava lakes from the discovery to the present. *Acta Vulcanologica*, *14*(15), 137–144.

Evernden, J. F. (1969). Identification of earthquakes and explosions by use of teleseismic data. *Journal of Geophysical Research (1896-1977)*, *74*(15), 3828–3856. https://doi.org/10.1029/JB074i015p03828

Francis, P., Oppenheimer, C., & Stevenson, D. (1993). Endogenous growth of persistently active volcanoes. *Nature*, *366*(6455), 554–557. https://doi.org/10.1038/366554a0

Geirsson, H., d'Oreye, N., Mashagiro, N., Syauswa, M., Celli, G., Kadufu, B., et al. (2017). Volcano-tectonic deformation in the Kivu Region, Central Africa: Results from six years of continuous GNSS observations of the Kivu Geodetic Network (KivuGNet). *Journal of African Earth Sciences*, *134*(2017), 809–823. https://doi.org/10.1016/j.jafrearsci.2016.12.013

Geirsson, H., D'Oreye, N., Nobile, A., Smets, B., & Kervyn, F. (2019). Deformation of tectonic and volcanic origin in the greater Kivu region. In A.Oth, & N.D'Oreye (Eds.), *Paper presented at the 100th Journées Luxembourgeoises de Géodynamique* (pp. 25–27). Luxembourg.

Georiska. (2021). *Nyiragongo's lava lake activity resumes*. Retrieved from https://georiska.africamuseum.be/en/news/NyiragongoLavaLakeActivity

Global Volcanism Program. (2021). Report on Nyiragongo (DR Congo). In K. L.Bennis, & E.Venzke (Eds.), *Bulletin of the global volcanism network* (Vol. 46, p. 6). Smithsonian Institution. https://doi.org/10.5479/si.GVP.BGVN202106-223030

Goldstein, T., & Osher, S. (2009). The Split Bregman method for L1-regularized problems. *SIAM Journal on Imaging Sciences*, *2*(2), 323–343. https://doi.org/10.1137/080725891

Huppert, H. E., & Hallworth, M. A. (2007). Bi-directional flows in constrained systems. *Journal of Fluid Mechanics*, *578*(May), 95–112. https://doi.org/10.1017/S0022112007004661

Kavotha, K. S., Mavonga, T., Durieux, J., & Mukambilwa, K. (2002). Towards a more detailed seismic picture of the January 17th, 2002 Nyiragongo eruption. *Acta Vulcanologica*, *14*(15), 87–100.

Komorowski, J.-C., Tedesco, D., Kasereka, M., Allard, P., Papale, P., Vaselli, O., et al. (2002). The January 2002 flank eruption of Nyiragongo volcano (Democratic Republic of Congo): Chronology, evidence for a tectonic rift trigger, and impact of lava flows on the city of Goma. *Acta Vulcanologica*, *14*(15), 27–62.

La Spina, G., Arzilli, F., Llewellin, E. W., Burton, M. R., Clarke, A. B., de' Michieli Vitturi, M., et al. (2021). Explosivity of basaltic lava fountains is controlled by magma rheology, ascent rate and outgassing. *Earth and Planetary Science Letters*, *553*, 116658. https://doi.org/10.1016/j.epsl.2020.116658

Lev, E., Ruprecht, P., Oppenheimer, C., Peters, N., Patrick, M., Hernández, P. A., et al. (2019). A global synthesis of lava lake dynamics. *Journal of Volcanology and Geothermal Research*, *381*, 16–31. https://doi.org/10.1016/j.jvolgeores.2019.04.010

Micchelli, C. A., Shen, L., & Xu, Y. (2011). Proximity algorithms for image models: Denoising. *Inverse Problems*, *27*(4). https://doi.org/10.1088/0266-5611/27/4/045009

Moore, C., Wright, T., Hooper, A., & Biggs, J. (2019). The 2017 Eruption of Erta 'Ale Volcano, Ethiopia: Insights into the shallow axial plumbing system of an incipient mid-ocean ridge. *Geochemistry, Geophysics, Geosystems*, *20*(12), 5727–5743. https://doi.org/10.1029/2019GC008692

Morrison, A., Whittington, A., Smets, B., Kervyn, M., & Sehlke, A. (2020). The rheology of crystallizing basaltic lavas from Nyiragongo and Nyamuragira volcanoes. *D.R.C. Volcanica*, *3*(1), 1–28. https://doi.org/10.30909/vol.03.01.0128

Oth, A., Barrière, J., D'Oreye, N., Mavonga, G., Subira, J., Mashagiro, N., et al. (2017). KivuSNet: The first dense broadband seismic network for the Kivu Rift region (Western branch of East African Rift). *Seismological Research Letters*, *88*(1), 49–60. https://doi.org/10.1785/0220160147

Patrick, M. R., Anderson, K. R., Poland, M. P., Orr, T. R., & Swanson, D. A. (2015). Lava lake level as a gauge of magma reservoir pressure and eruptive hazard. *Geology*, *43*(9), 831–834. https://doi.org/10.1130/G36896.1

Patrick, M. R., Houghton, B. F., Anderson, K. R., Poland, M. P., Montgomery-Brown, E., Johanson, I., et al. (2020). The cascading origin of the 2018 Kīlauea eruption and implications for future forecasting. *Nature Communications*, *11*(1), 1–13. https://doi.org/10.1038/s41467-020-19190-1

Patrick, M. R., Swanson, D., & Orr, T. (2019). A review of controls on Lava Lake level: Insights from Halema'uma'u Crater, Kīlauea Volcano. *Bulletin of Volcanology*, *81*(3), 13. https://doi.org/10.1007/s00445-019-1268-y

Pinel, V., Poland, M. P., & Hooper, A. (2014). Volcanology: Lessons learned from synthetic aperture radar imagery. *Journal of Volcanology and Geothermal Research*, *289*, 81–113. https://doi.org/10.1016/j.jvolgeores.2014.10.010

Poiata, N., Satriano, C., Vilotte, J. P., Bernard, P., & Obara, K. (2016). Multiband array detection and location of seismic sources recorded by dense seismic networks. *Geophysical Journal International*, *205*(3), 1548–1573. https://doi.org/10.1093/gji/ggw071

Pottier, Y. (1978). Première éruption historique du Nyiragongo et manifestations adventives simultanées du Volcan Nyamulagira (Chaîne des Virunga-Kivu-Zaire: Décembre 76-Juin 77). *Musée Royal de l'Afrique Centrale (Tervuren, Belgium), Rapport Annuel* (pp. 157–175).

Pouclet, A., & Bram, K. (2021). Nyiragongo and Nyamuragira: A review of volcanic activity in the Kivu rift, western branch of the East African Rift System. *Bulletin of Volcanology*, *83*(2), 10. https://doi.org/10.1007/s00445-021-01435-6

Rudin, L. I., Osher, S., & Fatemi, E. (1992). Nonlinear total variation based noise removal algorithms. *Physica D: Nonlinear Phenomena*, *60*(1–4), 259–268. https://doi.org/10.1016/0167-2789(92)90242-F

Rupnik, E., Pierrot-Deseilligny, M., & Delorme, A. (2018). 3D reconstruction from multi-view VHR-satellite images in MicMac. *ISPRS Journal of Photogrammetry and Remote Sensing*, *139*, 201–211. https://doi.org/10.1016/j.isprsjprs.2018.03.016

Rupnik, E., Pierrot Deseilligny, M., Delorme, A., & Klinger, Y. (2016). Refined satellite image orientation in the free open-source photogrammetric tools APERO/MICMAC. *ISPRS Annals of the Photogrammetry, Remote Sensing and Spatial Information Sciences*, *III-1*, 83–90. https://doi.org/10.5194/isprs-annals-III-1-83-2016

Smets, B. (2016). *Dynamics of volcanic activity in a youthful extensional setting studied by means of remote sensing and ground-based monitoring techniques: Nyiragongo and Nyamulagira volcanoes (North Kivu, D.R. Congo)*. Vrije Universiteit Brussel.

Smittarello, D., Barrière, J., D'Oreye, N., Smets, B., Oth, A., Shreve, T., et al. (2021). Propagation and arrest of the May 2021 lateral dike intrusion at Nyiragongo (D.R. Congo). *Paper presented at the AGU 2021 fall meeting*. New Orleans, LA. https://doi.org/10.1002/essoar.10509249.1

Stevenson, D. S., & Blake, S. (1998). Modelling the dynamics and thermodynamics of volcanic degassing. *Bulletin of Volcanology*, *60*(4), 307–317. https://doi.org/10.1007/s004450050234

Tanaka, K. (1983). Seismicity and focal mechanism of the volcanic earthquakes in the Virunga volcanic region. In H.Hamaguchi (Ed.), *Volcanoes Nyiragongo and Nyamuragira: Geophysical aspects* (The Facult, pp. 19–28). Sendai, Japan.

Tapete, D., Cigna, F., & Donoghue, D. N. M. (2016). "Looting marks" in space-borne SAR imagery: Measuring rates of archaeological looting in Apamea (Syria) with TerraSAR-X Staring Spotlight. *Remote Sensing of Environment*, *178*, 42–58. https://doi.org/10.1016/j.rse.2016.02.055

Tedesco, D., Vaselli, O., Papale, P., Carn, S. A., Voltaggio, M., Sawyer, G., et al. (2007). January 2002 volcano-tectonic eruption of Nyiragongo volcano, Democratic Republic of Congo. *Journal of Geophysical Research*, *112*, B09202. https://doi.org/10.1029/2006JB004762

Waldhauser, F., & Ellsworth, W. L. (2000). A double-difference earthquake location algorithm: Method and application to the Northern Hayward Fault, California. *Bulletin of the Seismological Society of America*, *90*(6), 1353–1368. https://doi.org/10.1785/0120000006

Wauthier, C., Cayol, V., Kervyn, F., & D'Oreye, N. (2012). Magma sources involved in the 2002 Nyiragongo eruption, as inferred from an InSAR analysis. *Journal of Geophysical Research: Solid Earth*, *117*(5), 1–20. https://doi.org/10.1029/2011JB008257

Wauthier, C., Smets, B., & Keir, D. (2015). Diking-induced moderate-magnitude earthquakes on a youthful rift border fault: The 2002 Nyiragongo-Kalehe sequence, D.R. Congo. *Geochemistry, Geophysics, Geosystems*, *16*(12), 4280–4291. https://doi.org/10.1002/2015GC006110

Witter, J. B., Kress, V. C., Delmelle, P., & Stix, J. (2004). Volatile degassing, petrology, and magma dynamics of the Villarrica Lava Lake, Southern Chile. *Journal of Volcanology and Geothermal Research*, *134*(4), 303–337. https://doi.org/10.1016/j.jvolgeores.2004.03.002

Wright, R., & Flynn, L. P. (2003). Satellite observations of thermal emission before, during, and after the January 2002 eruption of Nyiragongo. *Acta Vulcanologica*, *14*(1/2), 67. Retrieved from http://www.higp.hawaii.edu/lwright/acta15.pdf

References From the Supporting Information

Beckett, F. M., Burton, M., Mader, H. M., Phillips, J. C., Polacci, M., Rust, A. C., & Witham, F. (2014). Conduit convection driving persistent degassing at basaltic volcanoes. *Journal of Volcanology and Geothermal Research*, *283*, 19–35. https://doi.org/10.1016/j.jvolgeores.2014.06.006

Bonvalot, S., Remy, D., Deplus, C., Diament, M., & Gabalda, G. (2008). Insights on the March 1998 eruption at Piton de la Fournaise volcano (La Réunion) from microgravity monitoring. *Journal of Geophysical Research: Solid Earth*, *113*(5), 1–20. https://doi.org/10.1029/2007jb005084

Kettlety, T., Verdon, J. P., Werner, M. J., & Kendall, J. M. (2020). Stress transfer from opening hydraulic fractures controls the distribution of induced seismicity. *Journal of Geophysical Research: Solid Earth*, *125*(1). https://doi.org/10.1029/2019jb018794